



HAL
open science

Observed tracer fields structuration by mid-depth zonal jets in the tropical Pacific 2 Enzo Gronchi

Audrey Delpéch, Sophie Cravatte, Frédéric Marin, Yves Morel, Enzo Gronchi,
Elodie Kestenare

► To cite this version:

Audrey Delpéch, Sophie Cravatte, Frédéric Marin, Yves Morel, Enzo Gronchi, et al.. Observed tracer fields structuration by mid-depth zonal jets in the tropical Pacific 2 Enzo Gronchi. *Journal of Physical Oceanography*, 2020, 50 (2), pp.281-304. 10.1175/JPO-D-19-0132.1 . hal-03001946

HAL Id: hal-03001946

<https://hal.science/hal-03001946>

Submitted on 12 Nov 2020

HAL is a multi-disciplinary open access archive for the deposit and dissemination of scientific research documents, whether they are published or not. The documents may come from teaching and research institutions in France or abroad, or from public or private research centers.

L'archive ouverte pluridisciplinaire **HAL**, est destinée au dépôt et à la diffusion de documents scientifiques de niveau recherche, publiés ou non, émanant des établissements d'enseignement et de recherche français ou étrangers, des laboratoires publics ou privés.

1 **Observed tracer fields structuration by mid-depth zonal jets in the tropical**

2 **Pacific**

3 Audrey Delpech*, Sophie Cravatte, Frédéric Marin and Yves Morel

4 *Laboratoire d'Etudes Géophysiques et d'Océanographie Spatiale, LEGOS - UMR 5566*

5 *CNRS/CNES/IRD/UPS, Toulouse, France*

6 Enzo Gronchi

7 *Limnological Institute, University of Konstanz, Konstanz, Germany*

8 Elodie Kestenare

9 *Laboratoire d'Etudes Géophysiques et d'Océanographie Spatiale, LEGOS - UMR 5566*

10 *CNRS/CNES/IRD/UPS, Toulouse, France*

11 *Corresponding author address: LEGOS, 14 avenue Edouard Belin, Toulouse, France.

12 E-mail: audrey.delpech@legos.obs-mip.fr

ABSTRACT

13 The mid-depth ocean circulation in the tropical Pacific is dominated by sets
14 of alternating eastward and westward jets. The origin and transport properties
15 of these flow features remain in many ways an open question, all the more
16 crucial since their usual underestimation in ocean global circulation model
17 has been identified as a potential bias for the misrepresentation of the oxygen
18 minimum zones. In this study, we analyze the water mass properties asso-
19 ciated with these systems of jets using velocity and hydrographic sections.
20 Data acquired during a dedicated cruise carried out in the western part of the
21 basin and supplemented by cross-equatorial sections from historical cruises
22 in the central and eastern parts are analyzed. While it is confirmed that the
23 near-equatorial jets carry oxygen anomalies, contributing to the ventilation
24 of the eastern tropical Pacific, the data also revealed unexpected features.
25 Tracer distributions (oxygen, salinity and potential vorticity) show the pres-
26 ence of fronts extending from 500 to 3000 m and flanked by homogeneous
27 regions. These structures define meridional staircase profiles which coincide
28 with the alternating velocity profiles. Historical data confirm their presence
29 in the off-equatorial deep tropical ocean with a zonal and temporal coherence
30 throughout the basin. These observations support existing theoretical studies
31 involving homogenization by isopycnic turbulent mixing in the formation of
32 staircase profiles and maintenance of zonal jets. The effect of other processes
33 on the equilibration of tracer structures is also discussed.

34 **1. Introduction**

35 Observation of the intermediate and deep ocean circulation is quite challenging because, un-
36 like the surface currents that have been intensively studied thanks to satellite observations and
37 other near-surface measurements (surface drifters, buoys, underway ship measurements), deeper
38 observations are costly and sparse.

39 Our knowledge of this circulation in the tropical oceans has thus long been grounded on sections
40 from hydrographic cruises mostly limited to a few degrees off the equator (Firing et al. 1998). In
41 the tropical Pacific, pioneer cruises (Tsuchiya 1975; Eriksen 1981; Firing 1987; Firing et al. 1998;
42 Rowe et al. 2000; Gouriou et al. 2001) revealed the presence of several persistent zonal currents
43 below the thermocline in the near-equatorial band. Among them, the Tsuchiya jets are eastward
44 currents found in the whole basin just below the thermocline between 2.5° and 5° degrees from
45 the equator, with intensities of $20\text{-}40\text{ cm s}^{-1}$ (Rowe et al. 2000). The North and South Equatorial
46 Intermediate Countercurrent (NICC, SICC respectively) are weaker and deeper eastward currents
47 surrounding the westward L-EIC (Lower Equatorial Intermediate Current). They have been ob-
48 served at different longitudes across the basin at 2° from equator and below 600 m. On their
49 poleward side, the westward North and South Equatorial Intermediate currents (NEIC, SEIC re-
50 spectively) are found at 3° . In addition to these meridionally-alternating zonal currents, vertically-
51 alternating eastward and westward jets, called Equatorial Deep Jets (EDJs), are also found on the
52 equator within 1° (Ponte and Luyten 1989; Johnson et al. 2002), see also Fig. 1.

53 The advent of the Argo program provided a more comprehensive view with a basin-scale
54 coverage. The 1000 m mean velocity maps deduced from Argo float drifts at their parking
55 depth showed the zonal continuity of the L-EIC, SICC, NICC, NEIC and SEIC and revealed that
56 these currents are part of a broader system of meridionally-alternating zonal jets extending to at

57 least 15° off-equator (Ascani et al. 2010; Cravatte et al. 2012; Ollitrault and Colin de Verdière
58 2014). Absolute geostrophic mean currents obtained from gridded temperature and salinity Argo
59 products allowed the description of the vertical structure of these zonal currents in the whole
60 tropical band from the surface to 2000 m depth (Qiu et al. 2013b; Cravatte et al. 2017). The
61 arrival of new S-ADCP (Shipboard Acoustic Doppler Current Profilers) instruments with deeper
62 range also extended our ability to observe subsurface currents to more than 1000 m depth (Qiu
63 et al. 2017; Cravatte et al. 2017).

64

65 From all these studies, our current knowledge of the deep tropical Pacific Ocean circulation,
66 can be summarized as follows (see also Ménesguen et al. (2019) and Galperin and Read (2019,
67 chapter 3) for recent reviews). The mean circulation appears to be organized in three main systems
68 of zonal jets (Fig. 1 and Table 1):

- 69 • The Low-Latitude Subsurface Currents (LLSCs) are meridionally-alternating zonal currents
70 found between the thermocline and about 800 m depth, from the equator to about 18° , in-
71 cluding the well-studied Tsuchiya jets, also called NSCC and SSCC (Northern and Southern
72 Subsurface Countercurrents) (Tsuchiya 1975). Their velocity reaches 20 to 40 cm s^{-1} in the
73 core of the Tsuchiya jets but strongly decreases poleward. All these currents tend to get less
74 dense from west to east and denser and deeper from the equator poleward (Rowe et al. 2000;
75 Cravatte et al. 2017).
- 76 • The Low-Latitude Intermediate Currents (LLICs) are an apparently distinct set of
77 meridionally-alternating zonal currents, found from 700 m to at least 2000 m. Near the equa-
78 tor, this set includes the L-EIC, the SEIC and NEIC, and the SICC and NICC. The velocity
79 of these currents reaches 10 cm s^{-1} and they change sign every 1.5° (Cravatte et al. 2017).

80 • The Equatorial Deep Jets (EDJs) are equatorially-trapped, vertically-alternating zonal jets
81 with an amplitude of 10 cm s^{-1} and vertical wavelength close to 350 m (Leetmaa and Spain
82 1981). They are found to slowly propagate vertically with a period most recently estimated
83 around 12 years (Youngs and Johnson 2015).

84 These currents are clearly visible and identifiable on time-averaged sections but not necessarily
85 on snapshots where large differences from one cruise to another can be observed (Gouriou et al.
86 2006; Cravatte et al. 2017). Indeed, the equatorial region is subject to strong variability on many
87 time scales. The predominant and best documented variability is at seasonal timescales: it is
88 explained by the westward and downward propagation of an annual Rossby wave (Lukas and
89 Firing 1985; Kessler and McCreary 1993) that can seasonally induce a reversal of the currents in
90 the 2°S - 2°N band (Marin et al. 2010; Cravatte et al. 2012). Variability also exists at intraseasonal
91 and interannual timescales but is much less documented.

92
93 Despite this progress in our description of the intermediate and deep circulation, our knowledge
94 of these jets structures, their variability and properties is still far from being comprehensive, and
95 several questions remain open.

96
97 The first unresolved question concerns the dynamics of these jets, and the processes leading
98 to their formation and equilibration. Early studies attempted to explain the formation of the first
99 Tsuchiya jets independently, invoking different mechanisms (Johnson and Moore 1997; McCreary
100 et al. 2002; Hua et al. 2003; Marin et al. 2003; Furue et al. 2007, 2009). Later, two theoretical
101 frameworks have been proposed to explain the formation of systems of alternating zonal jets
102 (Ménésguen et al. 2019). In the first one, the main source of energy is coming from waves

103 (either equatorially-trapped waves or mid-latitudes waves). Jets can be seen either as the result
104 of instability of particular waves (Gill 1974; Hua et al. 2008; Ménesguen et al. 2009; d’Orgeville
105 et al. 2007; Ascani et al. 2010, 2015) or non-linear interactions and wave destabilization (Qiu
106 et al. 2013a). The second one explains the emergence of such zonal structures as a result of
107 the anisotropic inverse turbulent energy cascade on a beta plane (Rhines 1975; Berloff et al.
108 2009), extended to the equatorial regions in Theiss (2004). None of these studies have been
109 able to account for the complexity of the zonal and vertical structures of the three systems of
110 jets. Moreover, most Ocean General Circulation Models (OGCMs) are not able to correctly
111 simulate their structures and amplitudes, underlining that their formation mechanism is not fully
112 understood.

113

114 The second unresolved question concerns the role of these jets in the redistribution of water
115 properties across the Pacific Ocean. The misrepresentation of the intermediate circulation in
116 biogeochemical coupled OGCMs used in climate studies has been identified as a potential expla-
117 nation for the bias in oxygen and nutrients concentration in the eastern equatorial Pacific (Dietze
118 and Löptien 2013; Cabré et al. 2015) and in the Atlantic (Duteil et al. 2014). Some eastward jets
119 advect oxygen-rich waters to the east, and contribute to the ventilation of the Oxygen Minimum
120 Zones (OMZ), found in the eastern tropical oceans from 100 to 900 m depth (Karstensen et al.
121 2008). For instance, Tsuchiya (1981) showed that the southern Tsuchiya jet carries oxygen-rich
122 waters, originating from the Tasman sea and reaching the equatorial band through the Coral and
123 Solomon seas. Wyrcki and Kilonsky (1984) were then the first to show from in-situ observations
124 a zonal signature of oxygen in the core of the EUC flowing inside the thermocline (300 m) from
125 western well-ventilated regions to the eastern OMZ in the Pacific ocean. Using hydrographic
126 and current observations provided by cross-equatorial meridional sections of the World Ocean

127 Circulation Experiment (WOCE) and the Tropical Ocean-Atmosphere (TAO) project, Stramma
128 et al. (2010) observed that in the central and eastern tropical Pacific Ocean (from 170°W to
129 95°W), eastward subsurface currents (EUC, NSCC, SSCC, sSSCC) carry oxygen anomalies of
130 10-50 $\mu\text{mol kg}^{-1}$ with respect to their neighboring westward currents (SEC, EIC). Similar results
131 have been found in the Atlantic Ocean (Stramma et al. 2005, 2008, 2010; Brandt et al. 2008,
132 2012, 2015). These findings have also been confirmed by numerical simulations, which showed
133 that EUC, SSCC and sSSCC are crucial for the ventilation of oxygen minimum zones in both
134 tropical Atlantic (Duteil et al. 2014) and Pacific (Montes et al. 2014) oceans. Further off the
135 equator, Czeschel et al. (2015) suggested that LLSCs have also a signature in oxygen in the far
136 eastern Pacific.

137 At greater depths, there are fewer studies and most concern the Atlantic Ocean. The eastward
138 EDJs have been shown to transport oxygen in the Atlantic (Brandt et al. 2008, 2012). Because
139 of the oscillating nature of the EDJs at periods around 4.5 years in the Atlantic, and the expected
140 phase lag between the eastward currents and the oxygen concentrations, oxygen maxima in
141 eastward jets are not necessarily seen in snapshot measurements. The off-equatorial NICC has
142 also been identified as a potential supply path of oxygen-rich waters toward the north Atlantic
143 OMZ (Stramma et al. 2005). In the Pacific Ocean, there are hints that the upper parts of the NICC
144 and SICC may also supply oxygen eastward in the central and eastern parts of the basin (Stramma
145 et al. 2010). However, the signature in oxygen of the intermediate and deeper jets in the western
146 part of the basin has never been analyzed, and a global assessment of the three systems of zonal
147 jets and the properties they carry across the basin is still missing.

148

149 The purpose of the present article is to document the structures of tracer fields in zonal jets in
150 the Tropical Pacific. The study is based on observations from a dedicated cruise in the western

151 Equatorial Pacific, CASSIOPEE, supplemented by high-resolution, cross-equatorial sections from
152 historical cruises in the central and eastern part of the basin.

153

154 The paper is organized as follows: the datasets used as well as the methodology for the compu-
155 tations of some diagnostics are described in section 2. Section 3 presents the main results obtained
156 from the CASSIOPEE cruise, and reveals unexpected oxygen fronts in the eastward LLICs. Sec-
157 tion 4 checks the consistency of these findings in other historical cruises and Section 5 highlights
158 the contribution of these findings to our understanding of jets dynamics and their role in the redis-
159 tribution of water masses and tracers, in particular oxygen, at a basin scale.

160 **2. Data and methods**

161 This study is based on in-situ data analysis. This section provides a complete description of the
162 datasets and the post-processings used.

163 *a. CASSIOPEE cruise description*

164 The CASSIOPEE¹ oceanographic cruise took place onboard the french R/V L'Atalante in
165 2015 between July, 18 and August, 24. The main motivation of this cruise was to describe the
166 ocean circulation and water masses over the full depth of the ocean in the western equatorial
167 Pacific. During the cruise, surface-to-bottom measurements of currents and properties have been
168 acquired at 71 hydrological stations along 3 high-resolution meridional sections: one at 165°E
169 between 10°S and 2°N with a meridional resolution of 0.33°, and two others between the Papua
170 New Guinea coast and 2°N with a meridional resolution of 0.5° respectively at 157.5°E and
171 at 152.5°E (see the cruise plan on Fig. 2). The 165°E section will be the reference section for

¹<https://doi.org/10.17600/15001200>

172 the description of currents and their properties. The 152.5°E and 157.5°E sections will be used
173 to investigate the zonal continuity of the currents and their properties. During this cruise, the
174 following measurements were performed:

175

176 **Currents**

177 Horizontal currents were recorded along the ship track with two Shipboard-ADCPs (S-ADCP)
178 OS-38 kHz and OS-150 kHz, with typical vertical ranges of 1100 m and 350 m respectively.
179 S-ADCP data were processed and calibrated using the CODAS software. Surface-to-bottom
180 profiles of velocities were additionally measured at each hydrological station with two Lowered
181 ADCP (L-ADCP) attached to the rosette. The configuration used comprised a downward-looking
182 150 kHz L-ADCP and an upward-looking 300 kHz L-ADCP. Data were processed with the
183 version 10.16 of the LDEO software, using time-averaged S-ADCP velocities during stations and
184 bottom-reference velocity profiles as external constraints for the inversion (Visbeck 2002). The
185 resulting vertical profiles of zonal and meridional velocities have a vertical resolution of 10 meters.

186

187 **Temperature, Salinity and Oxygen**

188 During the 71 stations, vertical profiles of temperature, salinity and dissolved oxygen were mea-
189 sured from the surface to the bottom using two 24-Hz CTD (SBE911+ sensor) mounted on the
190 rosette. CTD data were corrected and adjusted to the salinity samples with the CADHYAC soft-
191 ware (Kermabon et al. 2015) and reduced to a 1 meter vertical resolution. Dissolved oxygen
192 sensor data were adjusted by comparison with a Winkler titration determination of water samples
193 (Langdon 2010; Uchida et al. 2010; Saout Grit et al. 2015).

194 When needed, data were regridded using 1d-linear interpolation and smoothed using running
195 hanning filters of 50 m to reduce small-scale vertical noise.

196 *b. Supplementary historical cruises*

197 In order to extend the results found with the CASSIOPEE dataset, independent and complemen-
198 tary datasets from the World Ocean Circulation Experiment (WOCE) provided by the Clivar and
199 Carbon Hydrographic Data Office (CCHDO²) are considered. Only full-depth, cross-equatorial
200 and high-resolution (at least 0.5°) sections have been selected, except for the equatorial profiles.
201 The list of the cruise sections we used is given in Table 2.

202 In addition, data from the TAO project cruises given in Table 3, which contributed to maintaining
203 approximately 70 moorings in the equatorial Pacific, were used. On a few of these cruises, from
204 2004 to 2008, dissolved oxygen was additionally measured to 1000 m depth (Stramma et al. 2010).
205 Though not full-depth, these data are still relevant for this study, since they provide repeated cross-
206 equatorial meridional sections with temperature, salinity, dissolved oxygen and S-ADCP velocity.

207 *c. Climatology products*

208 **Argo velocity products**

209 The Argo-based deep displacement Atlas (ANDRO³, Ollitrault and Rannou (2013)) gives, for
210 each Argo float, an estimate of the velocity at the float parking depth between two dives, resulting
211 in an approximately 10-day averaged estimation. In addition, we used a product of mean absolute
212 geostrophic velocity, hereafter called the CR17 product (Cravatte et al. 2017). It is based on
213 two components: a vertical shear of zonal geostrophic velocity computed off and at the equator
214 following the method presented by Picaut and Tournier (1991), from a mean high-resolution Argo
215 gridded temperature and salinity climatology at 1/6° resolution (Roemmich and Gilson 2009);
216 and a mean 1000-m Argo drift as the reference velocity at 1000m for vertically integrating the

²<https://cchdo.ucsd.edu/>

³<https://doi.org/10.17882/47077>

217 geostrophic shear (Cravatte et al. 2012).

218

219 **Atlas of hydrological properties**

220 The CSIRO Atlas of Regional Seas (CARS⁴) provided by the Commonwealth Scientific and
221 Industrial Research Organisation (CSIRO) is a climatology of seasonal ocean hydrographic prop-
222 erties (temperature, salinity and oxygen). This climatology is particularly well adapted for the
223 south western Pacific ocean because it includes data from many regional cruises, moored arrays
224 and autonomous profilers (Ridgway et al. 2002).

225 *d. Computation of physical and thermodynamical variables*

226 Thermodynamical variables such as potential density, absolute salinity and conservative
227 temperature were computed thanks to the python toolbox Gibbs Sea Water (GSW-python⁵), which
228 implements the Thermodynamics Equations of State (UNESCO-IOC 2010).

229

230 Potential vorticity (PV) is a key quantity to analyze the dynamical properties of jets (Baldwin
231 et al. 2007). It is a conservative tracer under adiabatic conditions and can help to characterize
232 water masses. It was here computed for the CASSIOPEE cruise sections assuming the dynamics
233 is two-dimensional and neglecting the zonal derivative of meridional velocity.

234 Ertel's PV, taking into account Boussinesq approximation, can be expressed as (Müller 2006):

$$Q = (\boldsymbol{\xi} + \mathbf{f}) \cdot \frac{\nabla \gamma}{\rho_0}, \quad (1)$$

235 where $\boldsymbol{\xi}$ is the vorticity, \mathbf{f} the rotation of the Earth, γ the neutral density (McDougall 1988; Eden
236 and Willebrand 1999) and ρ_0 a reference in-situ density. Note that PV at rest is:

⁴<http://www.marine.csiro.au/~dunn/cars2009/>

⁵<https://teos-10.github.io/GSW-Python/intro.html>

$$Q_0 = f \frac{\partial_z \bar{\gamma}}{\rho_0} \quad (2)$$

237 with f the vertical component of the planetary vorticity and $\bar{\gamma}$ the neutral density profile at rest.
 238 PV at rest is dominated by the variation of stratification with depth. The isopycnic variation of
 239 Ertel's PV is thus masked by this strong background variation and not easy to analyse on vertical
 240 sections. However, alternative PV can be defined, having the same properties (Lagrangian conser-
 241 vation for adiabatic motions, inversion properties to derive the circulation associated with the PV
 242 distribution, under geostrophic assumption). Following Morel et al. (2019), we define a rescaled
 243 PV as:

$$Q^* = (\boldsymbol{\xi} + \mathbf{f}) \cdot \nabla (G(\gamma)), \quad (3)$$

244 where G is a function chosen so that Q_0^* does not depend on z . A simple solution is to choose G so
 245 that $G(\bar{\gamma}(z)) = z$ and $Q_0^* = f$. The rescaled PV has dimension of vorticity. It is difficult to evaluate
 246 the vertical profile associated with the ocean at rest, but rescaling by a typical density profile
 247 chosen among the observations yields the expected result and allows to get rid of the signature of
 248 the pycnocline. Here we have chosen the profiles at 6.66°S for section 165°E and at 4.33°S for
 249 section 157.5°E . Our results are not sensitive to the choice of these profiles.

250 **3. Zonal jets and tracer structures in the south western equatorial Pacific : the CASSIOPEE** 251 **cruise**

252 *a. Currents structure and variability*

253 The structure of the currents during the CASSIOPEE cruise is shown using the full-depth L-
 254 ADCP data (Fig. 3). Although these transects are snapshots of the ocean circulation, which is

255 known to vary on a large range of time scales (from diurnal to inter-annual), most of the important
256 features of the mean tropical circulation and its organization into zonal jets can be identified. They
257 are described below for the three sections, from the equator poleward and from the surface to the
258 bottom.

259 1) EQUATORIAL SYSTEM

260 At the equator, strong positive velocities (up to 1 m s^{-1}) are found in the upper layers down
261 to 300 m on all sections in a latitudinal band extending from 2.5°S to at least 2°N (Fig. 4a).
262 This is not typical of this region of the Warm Pool, where the mean surface current in August is
263 expected to be very weak (Reverdin et al. 1994). Note however, that the cruise coincides with the
264 development of the strongest El Niño event of the early 21st century and with a series of strong
265 westerly wind events (McPhaden 2015). This unusual upper-ocean velocity structure is likely
266 related to the anomalous wind forcing during the cruise (not shown).

267 In the thermocline, a core of positive velocity (about 50 cm s^{-1}) is found at 200-250 m depth in
268 all sections and extends from 1.5°S to 1.5°N (Fig. 4). This corresponds to the EUC (Johnson et al.
269 2002). Just below the EUC, a core of westward current (15 cm s^{-1}) is found from 250 to 400 m
270 between 1.5°S and 1.5°N at 157.5°E and 165°E . It corresponds to the EIC.

271 From 500 to 2500 m the flow on the equator is predominantly westward with speeds up to
272 20 cm s^{-1} , corresponding to the climatological L-EIC. Superimposed on this large-vertical-scale
273 westward flow is the smaller-scale EDJ pattern with a vertical wavelength of about 300 m and with
274 an amplitude of 6 to 12 cm s^{-1} (Ponte and Luyten 1989; Youngs and Johnson 2015). The EDJs
275 are most evident in the full velocity field at 157.5°E (Fig. 3a); their zonal continuity from there
276 to 165°E emerges when a vertical wavenumber band-pass filter is used to isolate them from the
277 larger vertical scale flow (Section 3b. 2).

278 2) EXTRA-EQUATORIAL SYSTEMS

279 Off the equatorial band and below the thermocline, Subsurface Counter Currents (SCCs) with
280 positive velocities above 20 cm s^{-1} are found at $2^\circ\text{S} - 400 \text{ m}$ and $5^\circ\text{S} - 500 \text{ m}$, also referred to as
281 primary and secondary Tsuchiya jets (Tsuchiya 1975; Gouriou and Toole 1993). The primary SCC
282 at 2°S is seen on sections 165°E and 157.5°E but not at 152.5°E . Indeed, it has been suggested
283 that it originates at the Solomon strait (Tsuchiya 1981) which is located at 156°E (just east of this
284 section). The secondary Tsuchiya jet is also visible on the two easternmost sections (165°E and
285 157.5°E). A core of eastward velocity of amplitude 12 cm s^{-1} is also seen at $10^\circ\text{S} - 500 \text{ m}$ deep
286 on section 165°E (Fig. 3).

287 At intermediate depths, six intermediate zonal jets are observed between 1.5°S and 10°S , with
288 eastward-flowing jets at 1.5°S , 4°S and 7°S and westward-flowing jets at 2.5°S , 6°S and 8°S ,
289 extending from 800 m down to 3000 m where the bottom topography allows it, slightly sloping
290 toward the equator with depth (Fig. 3a). These jets have a good zonal coherence and can be
291 followed on sections 157.5°E and 152.5°E from the western boundary. The eastward jets at 1.5°N
292 and 1.5°S are generally referred to as the NICC and SICC (Firing et al. 1998).

293 At greater depths (below 3000 m), the circulation appears more constrained by the local to-
294 pography. The eastward jet at 7°S extends down to 3500 m and seems to be channeled between
295 two local ridges at 8.5°S and 5.5°S . Intense instantaneous velocities (up to 15 cm s^{-1}) are still
296 observed at the bottom or along ridges.

297 3) COMPARISON WITH THE MEAN CLIMATOLOGY

298 Figure 3a-b compares the meridional sections of L-ADCP zonal velocities measured during the
299 CASSIOPEE cruise, and the corresponding sections of zonal absolute geostrophic velocities from
300 the CR17 product corresponding to the mean for August, the month of the cruise. Figure 3c shows

301 meridional profiles of zonal velocities averaged over the isopycnal layers $1027.0-1027.6 \text{ kg m}^{-3}$
302 (corresponding approximately to 500-1500 m) for the same products.

303 In the western part of the basin, where the cruise was carried out, the two systems of zonal
304 jets, the LLSC and the LLIC, are not clearly distinct, as it is the case further east (not shown).
305 They appear as continuous slanted features in meridional-depth sections. As described above,
306 the CASSIOPEE observations capture most of the mean subthermocline jets: the EIC, the first
307 and second Tsuchiya jets, but the third eastward LLSC current located at 8.5°S in the annual
308 climatology (Cravatte et al. (2017)) is not fully observed, although a local velocity extremum is
309 present (Fig. 3c). Below, the CASSIOPEE observations capture well the six mean intermediate
310 jets between 10°S and 1.5°S , both in position and amplitude. The strongest differences between
311 the currents observed during the CASSIOPEE cruise and the annual mean from Argo product is
312 observed near the equator, between 2°S and 2°N , in the depth range 500-1500 m, where velocities
313 are weak and variable in direction in the annual climatology but much stronger and westward
314 during the CASSIOPEE cruise and in August climatology (Fig. 3c, sections 157.5°E and 165°E).
315 Such a result is compatible with the presence of a strong seasonal cycle in zonal currents near the
316 equator as revealed by observations (Gouriou et al. 2006; Cravatte et al. 2012) or in models (Marin
317 et al. 2010). This seasonal cycle has been explained by the westward and downward propagation
318 of an annual Rossby wave, forced near the surface by the seasonally-varying wind stress (Lukas
319 and Firing 1985; Kessler and McCreary 1993). This wave induces large velocity anomalies with
320 energy propagating annually from the eastern upper layers to the western deep layers (see Marin
321 et al. (2010), their figure 10). High westward velocities are found around 160°E between 800
322 and 1400 m during the months of August and September. Weaker westward anomalies of a few
323 centimeters per second are also expected at $8^\circ\text{S}-10^\circ\text{S}$ in August, as more than one meridional
324 Rossby mode could be present (Cravatte et al. 2012). The annual Rossby waves thus explains why

325 stronger than average westward currents along the equator are observed during CASSIOPEE; it
326 may also partly explains the absence of an eastward current at 8.5°S.

327

328 *b. Tracer fields properties*

329 In order to understand the role of this circulation on the transport of water masses and tracers,
330 sections of oxygen, salinity and rescaled PV are presented in Figs. 4 and 5. Meridional profiles
331 of zonal velocities and tracer fields are further shown on isopycnal layers chosen to target the
332 cores of the different jets mentioned in Section 3a. This complementary diagnostic ensures that
333 the horizontal variations and frontal structures are not the results of local and transient phenomena
334 such as the sudden lifting of isopycnals due to the passage of internal gravity waves.

335 1) MAIN WATER MASSES

336 The different water masses of the southwestern tropical Pacific Ocean are recognizable in Figs.
337 4 and 5 from the oxygen and salinity distributions. Between the surface and the thermocline (in
338 the upper hundred meters of the three sections), oxygen-rich waters with concentrations above
339 $160 \mu\text{mol kg}^{-1}$ are characteristic of the saturated mixed layer in equilibrium with the atmosphere
340 (Fig. 4b). Within the thermocline, the central waters display a large range of oxygen content and
341 are more often characterized by a salinity maximum (above 35 psu), originating from the south-
342 eastern subtropics (Kessler 1999). Two major water masses with different signatures in salinity
343 and oxygen are found at intermediate depths: The high oxygen ($160 \mu\text{mol kg}^{-1}$), low salinity
344 (34.3-34.5 psu) modified Antarctic Intermediate Water (AAIW) located around 1000 m southward
345 of 5°S (Fig. 5a-b) and the Equatorial Waters (EqW) with oxygen minima and relatively higher
346 salinity content (34.5-34.6 psu) found between the themocline and 2500 m, between 5°S and 5°N.

347 The mixing region between the AAIW and EqW is found between 15°S and 5°S (Bostock et al.
348 2010), inducing a large-scale smooth meridional gradient of oxygen and salinity. Below 2000 m,
349 the oxygen content increases downward where the very slow northward flow of Antarctic Bot-
350 tom Water (AABW) and Circumpolar Deep Waters (CDW) brings high oxygen concentrations
351 originating from the southern ocean (Fieux and Webster 2017).

352 2) THE EQUATORIAL SYSTEM

353 Oxygen-rich waters ($140 \mu\text{mol kg}^{-1}$) are found in the thermocline inside the EUC on the three
354 sections of CASSIOPEE cruise (Fig. 4a-b). These observations confirm that this eastward-flowing
355 current carries oxygen-rich waters from the well-ventilated western boundary toward the less-
356 oxygenated eastern basin (Tsuchiya 1981; Stramma et al. 2010). The oxygen content of the EUC
357 is compatible with the concentrations reported by Stramma et al. (2010). Although they did not
358 sample the same longitudes, they found concentrations of $125 \mu\text{mol kg}^{-1}$ at 170°W (the western-
359 most section of their paper), decreasing eastward to $30 \mu\text{mol kg}^{-1}$ at 85°W.

360 Between the thermocline and 3000 m, lower concentrations of oxygen (70 to $90 \mu\text{mol kg}^{-1}$)
361 are found in the near-equatorial band 2°S - 2°N (Fig. 5b). The intensity of the oxygen minimum
362 is modulated with depth (as for the velocity, see Fig. 3a). This is very likely the signature of the
363 EDJs. Figure 6 shows the vertical anomalies profile in oxygen concentration and zonal velocity
364 at the equator for the three sections of CASSIOPEE cruise. Original data have been band-pass
365 filtered for vertical scales between 100 and 500 m to remove small-scale noise and large-scale
366 variations. Both the zonal velocity and oxygen anomalies oscillate with a vertical wavelength of
367 about 330 m, corresponding roughly to the vertical wavelength of the EDJs. These oscillations
368 are especially visible on sections 157.5°E and 152.5°E, with a clear zonal continuity of vertical
369 minima and maxima, and are intensified in the 500 - 1800 m layer. Eastward jets (positive zonal ve-

370 locity anomalies) are associated with positive oxygen concentration anomalies and westward jets
371 (negative zonal velocity anomalies) are associated with negative oxygen concentration anomalies.
372 The magnitude of the oxygen content difference between eastward and westward jets reaches 15
373 to $20 \mu\text{mol kg}^{-1}$ at 500 m and decreases with depth. While the EDJs signature is still visible in
374 zonal velocity signal below 2000 m, with anomalies of 5 cm s^{-1} on section 152.5°E , it is non- ex-
375 istent in the oxygen signal (this will be further discussed in Section 5). These results are generally
376 consistent with the findings of Brandt et al. (2012), who show that oxygen concentrations in the
377 equatorial Atlantic are following a large range of variability (up to $60 \mu\text{mol kg}^{-1}$) at a given depth
378 and exhibit oscillations compatible with the 4.5 years period of the EDJs in this region. To our
379 knowledge, evidence of such a signature in the equatorial Pacific had not been provided yet.

380 3) THE EXTRA-EQUATORIAL LLSCS SYSTEM

381 As discussed in the previous section, several meridionally-alternating eastward and westward
382 jets are found between the thermocline and 800 m on the CASSIOPEE sections. The properties of
383 these jets in terms of oxygen, salinity and PV can be inferred from Fig. 5 and from the vertically-
384 averaged tracer variations within isopycnal layers, defined to encompass each individual jet along
385 the 165°E section (Fig. 7).

386 Layer $1026.45 - 1026.7 \text{ kg m}^{-3}$ (Fig. 7a) encompasses the first Tsuchiya jet. The velocity maxi-
387 mum is found at 2.3°S (32 cm s^{-1}) and the oxygen maximum ($120 \mu\text{mol kg}^{-1}$) as well, supporting
388 the idea of a transport of oxygen-rich waters by the first Tsuchiya jet. In contrast, PV and salinity
389 both show the presence of a frontal structure at that latitude. Interestingly, a front is also visible
390 in oxygen poleward of the jet, separating off-equatorial waters with high oxygen content from
391 equatorial waters with lower oxygen content. This result is in agreement with Rowe et al. (2000),
392 which also shows a front in PV associated with the first Tsuchiya jet. The relative importance

393 of the arising structure (either as front or maximum) will be discussed with respect to large-scale
394 gradient and physical processes in Section 5.

395 Layer 1026.8 - 1027.05 kg m⁻³ (Fig. 7b) is the layer where the core of the second Tsuchiya
396 jet can be found. Its position is detected by maximum positive velocities at 5°S (20 cm s⁻¹). At
397 the same latitude as zonal velocity maxima, frontal structures are found in the three tracer fields.
398 Oxygen drops from 110 μmol kg⁻¹ south of the jet to 90 μmol kg⁻¹ north and salinity increases
399 from 34.62 to 34.64 psu. This jet is flanked north and south by westward currents where the tracer
400 fields display very homogeneous values between 9°S - 6°S and 4°S - 2°S.

401 4) THE EXTRA-EQUATORIAL LLICs SYSTEM

402 Meridionally-alternating eastward and westward zonal jets are also found below 800 m to the
403 bottom (Section 3a). The striking features on the oxygen sections are the existence of meridional
404 fronts extending over more than 2000 m (from 500 m down to 2500-3000 m) following the core
405 of eastward jets at 7°S and 4°S (Fig. 5a) and at 2°S (Fig. 7c-d) with the same tilt towards the
406 equator with depth as for the currents. Frontal structures are denoted through a convergence of
407 oxygen isopleths alternating with quite homogeneous regions. Here the oxygen values decrease
408 suddenly from 125 μmol kg⁻¹ to 110 μmol kg⁻¹ between 7.5°S and 7°S, remain around 110
409 μmol kg⁻¹ between 7°S and 4.5°S and change again from 110 to 90 μmol kg⁻¹ between 4.5°S
410 and 4°S (Fig. 5a). Interestingly, these frontal structures are also seen, though they are very weak,
411 in salinity sections in the 800 - 1000 m depth range corresponding to the core of AAIW salinity
412 minima (Fig. 5b). The quantification of salinity variations appears more clearly in Figs. 7c-d:
413 salinity increases of about 0.01 psu at 7°S and 4°S and of 0.005 psu at 2°S. This last value is
414 weak but still significant given the vertical integration of the signal. In between the fronts, salinity
415 presents homogeneous values with latitude. This shows that the core of the salinity minimum

416 coming from the AAIW is gradually eroded from south to north. Last, similar frontal structures
417 are also seen in the PV field. Superimposed on the large-scale PV meridional gradient, one can
418 notice the presence of three frontal structures at 7°S, 4°S and 2°S on section 165°E (right panel,
419 Fig. 5c) and at 2°S and 4°S on section 157.5°E (mid panel, Fig. 5c).

420 The corresponding averages in isopycnal layers 1027.2-1027.4 kg m⁻³ and 1027.49-1027.57
421 kg m⁻³ are shown in Fig. 7c-d. Note that because the LLICs are slanted with depth (Fig. 3a),
422 two different isopycnal layers are needed to describe their depth-dependence. Figures 7c-d show
423 the very good correlation between oxygen, salinity and PV. The three tracers present staircase
424 meridional variations (alternation of frontal and homogeneous regions) with fronts coinciding
425 with eastward jets cores and homogeneous regions with westward jets. As shown on the different
426 sections (Fig. 5), these structures remain zonally coherent as they are present on the three sections
427 with similar amplitudes.

428
429 CASSIOPEE cruise helped to determine the tracer field structures associated with zonal jets,
430 due to the high resolution of the cruise stations and the good quality of the full-depth L-ADCP
431 data. It highlighted in particular unexpected frontal structures colocated for all tracer fields studied
432 (oxygen, salinity and PV) in all eastward jets except for the oxygen in the EUC, Tsuchiya jets and
433 EDJs, where local maxima are found.

434 **4. Temporal and zonal coherence across the basin.**

435 The purpose of this section is to determine to what extent the tracer structures associated with
436 the mid-depth zonal jets during the CASSIOPEE cruise resemble those in the rest of the basin at
437 different periods. For this purpose, we compared the results of the previous section with meridional
438 profiles of oxygen and salinity in isopycnal layers taken from historical cruises in the whole basin

439 (see Section 2). Ten meridional sections were considered: 165°E (P13), 180° (P14), 170°W (P15),
440 155°W, 150°W (P16), 140°W, 135°W (P17), 125°W, 110°W (P18) and 95°W. The location and
441 details about each cruise are given in Tables 2 and 3 and Fig. 2. For each of them we used S-ADCP
442 or L-ADCP measurements, when available.

443 *a. The EDJ system*

444 As for the CASSIOPEE cruise, vertically-alternating anomalies in oxygen do exist above 1800
445 m at the equator and may be related to the presence of the EDJ system (Fig. 8). The anomalies
446 are much weaker below. They are of similar amplitude for the P13 and P15 cruises, west of the
447 dateline, and decrease eastward of the dateline. They are found to be highly variable : the depths
448 of the oxygen extrema vary from one cruise to another, though the vertical scale remains similar.
449 For example, at 170°W (P15), we observe a phase reversal between the 2009 and 2016 cruises
450 oxygen signal in the depth range 1000-1800 m. This is consistent with the vertically-propagating
451 characteristics of the EDJs. Given the approximate 12 years period, we do not expect signals
452 from different snapshot cruises to coincide but to have different phases, as noted by Brandt et al.
453 (2012) in the Atlantic. However, a single period of 12 years is hardly identifiable from Fig. 8. For
454 example, cruises P14, 1993 and P14, 2007 are recorded 14 years apart, and still the signals present
455 a phase opposition, which seems not consistent with a 12-year period. Moreover, the phase lag
456 between different signals are not depth-independent. This rather suggests that EDJs have a broad-
457 band vertical scale and phase propagation period.

458 *b. The LLSCs system (including the Tsuchiya jets) and upper SICC and NICC*

459 The characteristic densities of the LLSC jets cores strongly depend on latitude and longitude:
460 the cores of the multiple eastward LLSC jets are known to get denser as the thermocline deepens

461 poleward (Cravatte et al. 2017), while the cores of the first and second SSCC are observed to get
462 lighter as the thermocline shoals from west to east (Rowe et al. 2000). To take into account these
463 variations of density, we define isopycnal layers with respect to the jets position (Table 4).

464
465 Between 10°S and 10°N, the Tsuchiya jets are discernible with positive velocities around
466 20 cm s⁻¹ at all longitudes (Fig. 9). The NSCC and SSCC are found to shift poleward from
467 3°N and 3°S (respectively) in the western part of the basin (170°W), to 5°N and 5°S in the eastern
468 part (110°W) in agreement with Rowe et al. (2000). They are associated with oxygen maxima
469 (Fig. 9a) whose amplitudes remain quite constant until 140°W (corresponding to a local anomaly
470 of 50 μmol kg⁻¹) and decrease eastward (about 20 μmol kg⁻¹ at 110°W). The maximum is no
471 longer discernible at 95°W. The oxygen content is however stronger in the NSCC than in the
472 SSCC in the middle of the basin and can be variable from one cruise to another (for instance, at
473 125°W oxygen content in the northern Tsuchiya jet varies from 80 μmol kg⁻¹ for GP-106 to 30
474 μmol kg⁻¹ in GP-504). Note that the erosion of maxima in the Tsuchiya jets along their path to
475 the eastern boundary shows that not only advection but also other processes such as consumption,
476 diffusion or mixing are taking place (see Section 5). This is in agreement with the findings of
477 Stramma et al. (2010), who analyzed cross-equatorial oxygen sections and found oxygen content
478 of 60 μmol kg⁻¹ at 140°W, decreasing eastward to about 30 μmol kg⁻¹ at 95°W. The signature
479 in salinity of these Tsuchiya jets is quite different. The most noticeable feature is the presence of
480 a front within the northern Tsuchiya jet, visible at each longitude, where the salinity decreases
481 from 34.8 psu equatorward to 34.65 psu poleward of the front (Fig. 9b). This front is flanked by
482 homogeneous or slowly-varying regions and indicates the presence of a barrier to mixing between
483 northern and southern water masses. The salinity signature associated with the SSCC and sSSCC

484 is either too weak with respect to the precision of the measurements or not zonally coherent.

485

486 Deeper, the layer 1027.15-1027.25 kg m^{-3} encompasses the off-equatorial LLSC and the upper
487 NICC and SICC (Fig. 10 and Table 4). The NICC and SICC are found at 2° on each side of the
488 equator. They are especially visible in longitudes 160-170°E in Argo geostrophic velocities (black
489 curve in Fig. 10) and are measured by ADCP data throughout the basin. These jets coincide with
490 oxygen maxima with relative amplitude of about $20 \mu\text{mol kg}^{-1}$. Further off-equator, small-scale
491 features that can be related to the jets structures do exist and are superimposed on the large-scale
492 meridional variation of oxygen in this region. However, the observed profiles are very noisy and
493 no zonally coherent signal emerges. The jets themselves are relatively weak ($1\text{-}3 \text{ cm s}^{-1}$) and their
494 position is subject to a strong variability, which may drastically complicate the picture of tracer
495 structures on a single snapshot.

496 *c. The extra-equatorial LLICs system*

497 To evaluate the zonal and temporal coherence of LLICs structures throughout the tropical
498 Pacific basin, we plot all the meridional profiles on a single graph together with the CR17
499 mean zonal velocity (Section 2c) for the isopycnal layer 1027.4 - 1027.6 kg m^{-3} corresponding
500 approximately to the 1000 - 1400 m depth range (Fig. 11).

501 First, staircase profiles in oxygen and salinity are observed from 20°S to 10°N for all cruises
502 at these depths, with fronts of amplitude 15 to $20 \mu\text{mol kg}^{-1}$ (oxygen) and 0.005 to 0.01 psu
503 (salinity) alternating with homogeneous regions extending over about 2° of latitude. Secondly,
504 staircase profiles are very coherent from one cruise to another (independently of the longitude,
505 year and period of the year at which the data were recorded). Indeed, a front in oxygen is for
506 example found at 5°N at 110°W during the cruises P18, 1994 and P18, 2016 carried out 22 years

507 apart. This front was also found at 135°W in 1991 and at 150°W in 2015 and 1991. Another
508 front is found at 8°N during the same cruises. P13, 2011 and P15, 2001 both capture frontal
509 structures in oxygen and salinity at 1.5°S and 4° corresponding to the position of the SICC and
510 the second intermediate eastward jet (Fig. 11a-c). Similarly, frontal structures in oxygen and
511 salinity profiles are observed at 11°S, 14°S and 17°S in 2001 and 2009 at 170°W at the position of
512 eastward currents. Note that at these depths, unlike in the upper layers where they are associated
513 with maxima, the SICC and NICC are more associated with frontal structures. The meridional
514 distance between frontal structures is close to 3° in latitude, corresponding to the meridional
515 scale of the meridionally-alternating zonal jets. To highlight this relation, normalized spectrum of
516 the climatological Argo geostrophic velocity and tracer profiles in the same isopycnal layer are
517 plotted against the meridional wave number (Fig. 11d-e). Maximum power density is found at a
518 meridional wavenumber $k_y \simeq 0.33$, corresponding to a meridional wavelength of $\lambda_y \simeq 3^\circ$.

519

520 These observations confirm that while oxygen maxima are more associated with the near-
521 equatorial components of the zonal jet systems (EUC, Tsuchiya jets, EDJs), staircase profiles are a
522 general and permanent tracer structure associated with extra-equatorial and relatively deep (deeper
523 than 1000 m) zonal jets in the tropical Pacific ocean (LLICs). They show the spatial coincidence
524 of all tracer variations as staircase profiles, which consist in fronts inside eastward currents and
525 homogeneous properties inside westward currents.

526 **5. Discussion**

527 The aim of this section is to discuss the following points: (i) what do the observed tracer struc-
528 tures tell us about the dynamics of the zonal jets ? which process is able to homogenize tracers
529 at very specific locations and to create fronts in between, such as those observed in the core of

530 the eastward zonal LLICS jets ? (ii) what is the effect of the zonal circulation on the water mass
531 distribution and on the ventilation of the equatorial Pacific ?

532 *a. Do staircase profiles result from isopycnic mixing ?*

533 We discuss here isopycnic processes associated with zonal jets which may explain the observed
534 tracer structures: (i) zonal advection and (ii) turbulent diffusion (Fig. 13a-c). Zonal advection can
535 clearly explain the presence of minima and maxima observed in the core of some jets (Section 4b).
536 However, the generation of observed staircase profiles requires more complex dynamics than the
537 two aforementioned processes. Indeed, zonal advection can generate sharp fronts by straining
538 a property gradient field, but in this case the sharpened property gradients would coincide with
539 the maximum velocity shear, ie. in between the jets. Thus zonal advection, even in a slanting
540 gradient (Fig. 13b), cannot explain the location of frontal regions inside jets. In addition, it cannot
541 explain the regions of homogeneous property. Similar inconsistencies are found for the diffusion
542 and homogenization of tracers in closed gyres, as discussed by Rhines and Young (1982) for PV.
543 Closed gyres determine regions where tracers are confined and can be homogenized by horizontal
544 diffusion. The possibility that tropical mid-depth zonal jets may form recirculation gyres has been
545 discussed by Rowe et al. (2000) and Ascani et al. (2010). However this mechanism would result
546 in uniform tracer regions localized within pairs of eastward and westward jets forming a gyre
547 (Fig. 13c) and not within westward jets as observed. Thus, even if zonal advection and diffusion
548 associated with zonal jets play a role in the transport of tracers, these processes alone cannot
549 explain the observations.

550 Alternatively, staircase profiles might be explained by the existence of meridionally inhomoge-
551 neous isopycnic mixing, creating regions of uniform tracers flanked by regions of increased tracer
552 gradient (as described in Fig. 13d). In our case, mixing would be enhanced within westward jets

553 and inhibited within eastward jets, at the location of the fronts. The existence of such inhomogeneous isopycnic mixing is not unrealistic: it is consistent with theoretical studies and idealized numerical simulations of geophysical flows on a beta plane that explain how zonal jets can be maintained against dissipation. The principle is that if zonal jets do exist, they will necessarily be associated to PV variations. Isopycnal mixing will then be enhanced in regions where the PV gradient is weak and inhibited in regions where the PV gradient is strong (PV front), resulting in an inhomogeneous mixing and eventually the formation of staircases (McIntyre 1982; Baldwin et al. 2007; Dritschel and McIntyre 2008; Berloff et al. 2009; Dritschel and Scott 2011). It is important to note that such processes do not explain the generation of the zonal jets, but only their equilibration. Even though our analysis is not exhaustive, the similarity between all tracers profiles and the consistency of the frontal and homogeneous regions with the location of observed zonal jets (Sections 3 and 4) suggest that the localized mixing mechanism could be at the origin of the observed staircase profiles.

566 In addition, staircase structures remain coherent over a large part of the basin and over a period of at least 20 years (Fig. 11), supporting the idea that an equilibrium is reached between the processes at play. In particular, in the presence of a large-scale zonal gradient of properties, zonal advection by jets will create advective tracer anomalies (Fig. 13a), that have to be equilibrated by other processes. Possible additional mechanisms are, for example, the modification of large-scale vertical mixing by the vertical shear of the strongest jets may impact tracers distribution. The structuration of ecosystems by the jet dynamics could lead, in the case of the oxygen, to localized increased consumption regions, also modifying the meridional structure of oxygen. Increased concentrations of marine snow at the equator, between mid-depth eastward jets (the SICC and the NICC), has indeed been reported recently (Kiko et al. 2017). Finally, the mechanisms associated with the generation of the jets (see Ménesguen et al. 2019, and references therein) could also act

577 on tracers. A full understanding of the relative contributions of all these terms to maintain the
578 staircase structures would require a dedicated modelling study, and is beyond the scope of this
579 paper.

580 *b. What are the implications for the transport of water masses and the ventilation of the deep*
581 *ocean ?*

582 To better understand how waters may be transported or modified at basin-scale by the systems
583 of zonal jets, we need to examine the water masses present and their large-scale gradients.

584 The equatorial basin is filled from the thermocline to 2500 m and between 5°S and 5°N by the
585 Equatorial Waters (EqW), with horizontal homogeneous temperature and salinity properties (Fieux
586 and Webster 2017). Therefore, a salinity background gradient is primarily meridional and concen-
587 trated at and poleward of the EqW boundary (Fig. 12 b-d). It is thus not surprising that advective
588 anomalies within zonal jets do not show up for salinity but that staircases are present for the
589 Tsuchiya jets and the LLICs (Figs. 5, 9b and 11). Local homogenization processes, which grad-
590 ually lead to the transformation of the off-equatorial water masses to the equatorial water mass,
591 might then play an important role in the erosion of intermediate water masses in the tropics.

592 Unlike salinity, oxygen concentrations present strong contrasts at basin-scale in the tropical
593 Pacific, due to the presence of the OMZ in the eastern part of the basin and the supply of oxygen-
594 rich waters from the western boundary currents (Figs. 12a-c). Our observations show that the
595 oxygen signature depends on the different systems of jets.

596 The EUC, the first and second Tsuchiya jets carry oxygen-rich waters (Sections 3b and 4a-b).
597 The oxygen anomalies associated with the jets are observable from the western boundary (Figs. 4b
598 and 6), supporting the idea that the EUC and Tsuchiya jets are fed by the oxygen-rich waters from
599 the Solomon Sea in the upper and lower thermocline, as first suggested by Tsuchiya (Tsuchiya

600 1981). Given the width of the Pacific ocean (14500 km) and the speed of the zonal jets (5 cm s^{-1}),
601 the time needed for a particle to travel from west to east is about 9 years, long enough for turbulent
602 diffusion and biological processes to erode the oxygen anomaly from $120 \mu\text{mol kg}^{-1}$ at 165°E
603 to $40 \mu\text{mol kg}^{-1}$ at 95°W (Fig. 9a). Weak anomalies are still observed in the eastern Pacific,
604 suggesting that these jets are an important source of ventilation for the OMZ.

605 In the equatorial Pacific, the eastward EDJs and upper SICC and NICC are also associated with
606 oxygen anomalies (Figs. 8, 10) that have a larger amplitude in the western part of the basin and
607 above $\sim 1500 \text{ m}$. This raises the question of the main source of oxygen-rich waters transported
608 by these jets. Above 1200 m , the western boundary current carries oxygen-rich waters from the
609 southern ocean and might provide a source of ventilated waters to these eastward jets (see in
610 Fig. 5b section 157.5°W , the two western boundary stations). In addition, the presence of the
611 OMZ in the eastern part of the basin and in the upper 900 m provide a large-scale zonal gradient
612 (Fig. 12a) which likely enhances oxygen anomalies in the basin interior due to advective processes
613 (Fig. 13a). Deeper however, the large-scale background gradient is mainly meridional (Fig. 12c)
614 and the bathymetry can prevent direct supply from the western boundary. The Solomon Sea is
615 connected to the equator by two main pathways: the Vitiaz Strait (closed below 1200 m), and the
616 Solomon Strait, whose waters are blocked by a seamount reaching 2000 m depth located at 157°E .
617 An oxygen supply of the eastward jets (EDJs and S- NICC) by the western boundary current seems
618 thus more difficult below 2000 m . This may explain why there is no clear oxygen anomalies in
619 their cores.

620 In the off-equatorial LLSC system, oxygen signature is hard to detect and varies from one cruise
621 to another. This lack of coherency can have two explanations. First, the lack of coherency of
622 the jets themselves. Indeed, whereas EDJs, EUC and Tsuchiya jets are permanent features of
623 the circulation, off-equatorial LLSCs are weaker and subject to high variability (Cravatte et al.

624 2017; Qiu et al. 2013a). They may contribute to the ventilation more sporadically (Czeschel et al.
625 2011). Second, the background gradient has both zonal and meridional components at these depths
626 (Fig. 12a) and is prone to emphasize both advection and mixing mechanisms. The resulting tracer
627 pattern may thus look more complex.

628 Finally, in the LLIC system, below 1000 m, the jets are systematically associated with staircase
629 structures at different times and longitudes (Section 3b. 4 and 4c). Staircase profiles are compat-
630 ible with the observed meridional large-scale gradient in oxygen (Figs. 12c) in the presence of
631 isopycnic inhomogeneous mixing mechanisms (Fig. 13d).

632 **6. Conclusions and Perspectives**

633 Based on high-resolution in-situ data, this study aims at better describing the physical and hy-
634 drological properties associated with the jet-structured mid-depth tropical ocean circulation. Our
635 study has shown that (i) in agreement with previous studies, the close equatorial jets including the
636 EUC, first and second Tsuchiya jets, EDJs, upper NICC and SICC, are associated with oxygen
637 anomalies and transport oxygen-rich waters from the oxygen-rich western boundary (between the
638 thermocline and 1500 m) toward the OMZ in the eastern basin. This confirms the importance of
639 simulating them correctly in models aiming to accurately represent the OMZ ventilation processes.
640 In addition, this calls for a deeper investigation of the water sources for these jets. The sources of
641 the EUC have been well documented since the seminal paper by Tsuchiya et al. (1989) (Grenier
642 et al. 2011), but the pathways and precise origin of waters feeding the NICC, SICC and EDJs are
643 less documented and deserve further study. (ii) In the off-equatorial LLSC system, the signature
644 of the jets is more difficult to detect. Ventilation can occur intermittently but is much harder to
645 quantify because of the possible latent characteristic of these jets. Its precise quantification would
646 require more systematic measurements than scarce cruise transects. The increasing number of

647 Argo floats with oxygen sensors may open a perspective to pursue this work. (iii) In the deeper
648 LLICs, we have discovered, in the western Pacific, the presence of two sharp fronts, distant of
649 about 400 km from each other and extending over more than 2500 m (from 500 m down to 3000
650 m) for three tracers (potential vorticity, salinity and oxygen).

651 Investigating the zonal continuity of these frontal structures, we have found that they are ob-
652 served from 165°E to at least 110°W and from 20°S to 10°N at each location where an eastward
653 jet is observed, resulting in staircase meridional profiles. We have interpreted the presence of
654 these staircase profiles as the possible result of some localized mixing processes. This finding is
655 compatible with theories explaining the maintenance of zonal jets by turbulent mixing. Potential
656 vorticity staircases had already been predicted by these theoretical or numerical studies (McIntyre
657 2008). But it is the first time, that observations corroborate these theories in the ocean and extend
658 it to other tracers, supporting that isopycnal mixing is an effective process and a major ingredient
659 for the equilibration of the jets. We also suggested that LLICs do not contribute to ventilation by
660 direct advection. This does however not exclude an indirect role of these jets on the local oxygen
661 budget of the OMZ by mesoscale processes (mixing, eddy activity).

662 The different structuring of the tracer fields showing up sometimes as alternating minima and
663 maxima and sometimes as alternating frontal and uniform regions can possibly be explained by
664 the relative importance of the competitive mechanisms (advection and mixing) according to the
665 dominant background large-scale forcing gradient. But other mechanisms and in particular oxygen
666 consumption can also explain these differences, as high biological activity (respiration, degrada-
667 tion of organic matter) takes place. Finally, the permanence of the structures suggests that in any
668 cases, a long-term equilibrium must exist between the processes at play.

669 This study raises further questions on the consequences of the presence of mixing and large-
670 scale frontal structures in the deep ocean. It questions in particular the ability of these jets to

671 create barriers to meridional water masses transport, mixing and erosion, which could impact the
672 ocean heat budget, ecosystems or global overturning circulation (Baldwin et al. 2007; Kiko et al.
673 2017). The deep jets systems require thus increased attention as it may play a crucial role in
674 shaping oceanic landscape.

675 *Acknowledgments.* This work and the CASSIOPEE cruise ([https://doi.org/10.17600/](https://doi.org/10.17600/15001200)
676 15001200) were supported by the French national programme LEFE/INSU, within the project
677 ZEBRE. The authors deeply thank the crew of the R/V Atalante, and the engineers, especially
678 from the IRD US-IMAGO and DT-INSU team (F. Baurand, J. Grelet, F. Perault, E. de St-Leger,
679 P. Rousselot, N. Lamande, E. Morris, R. Heux) and scientists (G. Eldin, J. Verron, A. Ganachaud,
680 M. Duran, S. Lal, S. Durrieu de Madron, C. Grit-Saout) who carefully sampled, recorded, and
681 processed the data used in this paper during the CASSIOPEE cruise. They also wish to thank
682 Kristene MacTaggart and Gregory Johnson from NOAA/PMEL for providing the TAO cruises
683 oxygen data. The authors thank the CCHDO project (<https://cchdo.ucsd.edu/>) and the PIs
684 of the available cruises, that delivers high quality global hydrographic data, hence allowing data
685 to have multiple lives. This study has also been possible thanks to the amount of Argo data, col-
686 lected and made freely available by the International Argo Program and the national programs that
687 contribute to it. The Argo Program is part of the Global Ocean Observing System (Argo 2000).
688 The authors thank M. Ollitrault, J.-P. Ranou and other contributors for making the ANDRO Atlas
689 available (<https://doi.org/10.17882/47077>), and the CSIRO Marine Laboratories for mak-
690 ing the CARS climatology available. The authors are grateful to Eric Firing, who provided access
691 to L-ADCP data used in this study and insightful suggestions. They wish to deeply thank him and
692 an anonymous reviewer whose comments have significantly improved the manuscript. This work
693 also benefited from fruitful discussions with P. Brandt, L. Thomas and P. Haynes.

694 **References**

- 695 Ascani, F., E. Firing, P. Dutrieux, J. P. McCreary, and A. Ishida, 2010: Deep equatorial ocean
696 circulation induced by a forced–dissipated yanai beam. *J. Phys. Oceanogr.*, **40** (5), 1118–1142.
- 697 Ascani, F., E. Firing, J. P. McCreary, P. Brandt, and R. J. Greatbatch, 2015: The deep equatorial
698 ocean circulation in wind–forced numerical solutions. *J. Phys. Oceanogr.*, **45** (6), 1709–1734.
- 699 Baldwin, M. P., P. B. Rhines, H.-P. Huang, and M. E. McIntyre, 2007: The jet-stream conundrum.
700 *Science*, **315** (5811), 467–468.
- 701 Berloff, P., I. Kamenkovich, and J. Pedlosky, 2009: A mechanism of formation of multiple zonal
702 jets in the oceans. *J. Fluid Mech.*, **628**, 395–425.
- 703 Bostock, H. C., B. N. Opdyke, and M. J. Williams, 2010: Characterising the intermediate depth
704 waters of the pacific ocean using $\delta^{13}\text{C}$ and other geochemical tracers. *Deep Sea Research Part*
705 *I: Oceanographic Research Papers*, **57** (7), 847–859.
- 706 Brandt, P., V. Hormann, B. Bourlès, J. Fischer, F. A. Schott, L. Stramma, and M. Dengler,
707 2008: Oxygen tongues and zonal currents in the equatorial atlantic. *J. Geophys. Res.: Oceans*,
708 **113** (C4).
- 709 Brandt, P., and Coauthors, 2012: Ventilation of the equatorial atlantic by the equatorial deep jets.
710 *J. Geophys. Res.: Oceans*, **117** (C12).
- 711 Brandt, P., and Coauthors, 2015: On the role of circulation and mixing in the ventilation of oxygen
712 minimum zones with a focus on the eastern tropical north atlantic. *Biogeosciences*, **12**, 489–512.
- 713 Cabré, A., I. Marinov, R. Bernardello, and D. Bianchi, 2015: Oxygen minimum zones in the
714 tropical pacific across cmip5 models: mean state differences and climate change trends. *Bio-*
715 *geosciences*, **12** (18), 5429–5454.

716 Cravatte, S., W. S. Kessler, and F. Marin, 2012: Intermediate zonal jets in the tropical pacific ocean
717 observed by argo floats. *J. Phys. Oceanogr.*, **42** (9), 1475–1485.

718 Cravatte, S., E. Kestenare, F. Marin, P. Dutrieux, and E. Firing, 2017: Subthermocline and in-
719 termediate zonal currents in the tropical pacific ocean: Paths and vertical structure. *J. Phys.*
720 *Oceanogr.*, **47** (9), 2305–2324.

721 Czeschel, R., L. Stramma, F. U. Schwarzkopf, B. S. Giese, A. Funk, and J. Karstensen, 2011:
722 Middepth circulation of the eastern tropical south pacific and its link to the oxygen minimum
723 zone. *J. Geophys. Res.: Oceans*, **116** (C1).

724 Czeschel, R., L. Stramma, R. A. Weller, and T. Fischer, 2015: Circulation, eddies, oxygen and
725 nutrient changes in the eastern tropical south pacific ocean. *Ocean Science*, **11** (3), 455–470.

726 Dietze, H., and U. Lötjien, 2013: Revisiting nutrient trapping in global coupled biogeochemical
727 ocean circulation models. *Global Biogeochemical Cycles*, **27** (2), 265–284.

728 d’Orgeville, M., B. L. Hua, and H. Sasaki, 2007: Equatorial deep jets triggered by a large vertical
729 scale variability within the western boundary layer. *J. Mar. Res.*, **65** (1), 1–25.

730 Dritschel, D., and M. McIntyre, 2008: Multiple jets as pv staircases: the phillips effect and the
731 resilience of eddy-transport barriers. *Journal of the Atmospheric Sciences*, **65** (3), 855–874.

732 Dritschel, D., and R. Scott, 2011: Jet sharpening by turbulent mixing. *Philosophical Transac-*
733 *tions of the Royal Society of London A: Mathematical, Physical and Engineering Sciences*,
734 **369** (1937), 754–770.

735 Duteil, O., F. U. Schwarzkopf, C. W. Böning, and A. Oschlies, 2014: Major role of the equatorial
736 current system in setting oxygen levels in the eastern tropical atlantic ocean: A high-resolution
737 model study. *Geophys. Res. Lett.*, **41** (6), 2033–2040.

- 738 Eden, C., and J. Willebrand, 1999: Neutral density revisited. *Deep Sea Research Part II: Topical*
739 *Studies in Oceanography*, **46 (1-2)**, 33–54.
- 740 Eriksen, C. C., 1981: Deep currents and their interpretation as equatorial waves in the western
741 pacific ocean. *J. Phys. Oceanogr.*, **11 (1)**, 48–70.
- 742 Fieux, M., and F. Webster, 2017: *The planetary ocean*. Current natural sciences, EDP sciences.
- 743 Firing, E., 1987: Deep zonal currents in the central equatorial pacific. *J. Mar. Res.*, **45 (4)**, 791–
744 812.
- 745 Firing, E., S. E. Wijffels, and P. Hacker, 1998: Equatorial subthermocline currents across the
746 pacific. *J. Geophys. Res.: Oceans*, **103 (C10)**, 21 413–21 423.
- 747 Furue, R., J. P. McCreary Jr, and Z. Yu, 2009: Dynamics of the northern tsuchiya jet. *J. Phys.*
748 *Oceanogr.*, **39 (9)**, 2024–2051.
- 749 Furue, R., J. P. McCreary Jr, Z. Yu, and D. Wang, 2007: Dynamics of the southern tsuchiya jet. *J.*
750 *Phys. Oceanogr.*, **37 (3)**, 531–553.
- 751 Galperin, B., and P. L. Read, 2019: *Zonal Jets: Phenomenology, Genesis, and Physics*. Cambridge
752 University Press, 46-72 pp.
- 753 Gill, A., 1974: The stability of planetary waves on an infinite beta-plane. *Geophysical and Astro-*
754 *physical Fluid Dynamics*, **6 (1)**, 29–47.
- 755 Gouriou, Y., T. Delcroix, and G. Eldin, 2006: Upper and intermediate circulation in the western
756 equatorial pacific ocean in october 1999 and april 2000. *Geophys. Res. Lett.*, **33 (10)**.
- 757 Gouriou, Y., and J. Toole, 1993: Mean circulation of the upper layers of the western equatorial
758 pacific ocean. *J. Geophys. Res.: Oceans*, **98 (C12)**, 22 495–22 520.

- 759 Gouriou, Y., and Coauthors, 2001: Deep circulation in the equatorial atlantic ocean. *Geophys. Res.*
760 *Lett.*, **28 (5)**, 819–822.
- 761 Grenier, M., S. Cravatte, B. Blanke, C. Menkes, A. Koch-Larrouy, F. Durand, A. Mélet, and
762 C. Jeandel, 2011: From the western boundary currents to the pacific equatorial undercur-
763 rent: Modeled pathways and water mass evolutions. *Journal of Geophysical Research: Oceans*,
764 **116 (C12)**.
- 765 Hua, B. L., M. D’Orgeville, M. D. Fruman, C. Menesguen, R. Schopp, P. Klein, and H. Sasaki,
766 2008: Destabilization of mixed rossby gravity waves and the formation of equatorial zonal jets.
767 *J. Fluid Mech.*, **610**, 311–341.
- 768 Hua, B. L., F. Marin, and R. Schopp, 2003: Three-dimensional dynamics of the subsurface coun-
769 tercurrents and equatorial thermostad. part i: Formulation of the problem and generic properties.
770 *J. Phys. Oceanogr.*, **33 (12)**, 2588–2609.
- 771 Johnson, G. C., E. Kunze, K. E. McTaggart, and D. W. Moore, 2002: Temporal and spatial struc-
772 ture of the equatorial deep jets in the pacific ocean. *J. Phys. Oceanogr.*, **32 (12)**, 3396–3407.
- 773 Johnson, G. C., and D. W. Moore, 1997: The pacific subsurface countercurrents and an inertial
774 model. *J. Phys. Oceanogr.*, **27 (11)**, 2448–2459.
- 775 Karstensen, J., L. Stramma, and M. Visbeck, 2008: Oxygen minimum zones in the eastern tropical
776 atlantic and pacific oceans. *Progress in Oceanography*, **77 (4)**, 331–350.
- 777 Kermabon, C., L. B. P, and T. V, 2015: Cadyhac: Chaîne d’ajustage des donnes d’hydrologie aprs
778 campagne - documentation utilisateur (v1.1). r.int. ode/lpo/15-01. Tech. rep., IFREMER.
- 779 Kessler, W. S., 1999: Interannual variability of the subsurface high salinity tongue south of the
780 equator at 165 e. *J. Phys. Oceanogr.*, **29 (8)**, 2038–2049.

- 781 Kessler, W. S., and J. P. McCreary, 1993: The annual wind-driven rossby wave in the subthermo-
782 cline equatorial pacific. *J. Phys. Oceanogr.*, **23** (6), 1192–1207.
- 783 Kiko, R., and Coauthors, 2017: Biological and physical influences on marine snowfall at the
784 equator. *Nature Geoscience*, **10** (11), 852.
- 785 Langdon, C., 2010: Determination of dissolved oxygen in seawater by winkler titration using the
786 amperometric technique. Tech. rep.
- 787 Leetmaa, A., and P. F. Spain, 1981: Results from a velocity transect along the equator from 125 to
788 159 w. *J. Phys. Oceanogr.*, **11** (7), 1030–1033.
- 789 Lukas, R., and E. Firing, 1985: The annual rossby wave in the central equatorial pacific ocean. *J.*
790 *Phys. Oceanogr.*, **15** (1), 55–67.
- 791 Marin, F., E. Kestenare, T. Delcroix, F. Durand, S. Cravatte, G. Eldin, and R. Bourdalle-Badie,
792 2010: Annual reversal of the equatorial intermediate current in the pacific: Observations and
793 model diagnostics. *J. Phys. Oceanogr.*, **40** (5), 915–933.
- 794 Marin, F., R. Schopp, and B. L. Hua, 2003: Three-dimensional dynamics of the subsurface coun-
795 tercurrents and equatorial thermostad. part ii: Influence of the large-scale ventilation and of
796 equatorial winds. *J. Phys. Oceanogr.*, **33** (12), 2610–2626.
- 797 McCreary, J. P., P. Lu, and Z. Yu, 2002: Dynamics of the pacific subsurface countercurrents. *J.*
798 *Phys. Oceanogr.*, **32** (8), 2379–2404.
- 799 McDougall, T. J., 1988: Neutral-surface potential vorticity. *Progress in Oceanography*, **20** (3),
800 185–221.
- 801 McIntyre, M., 2008: Potential-vorticity inversion and the wave-turbulence jigsaw: some recent
802 clarifications. *Advances in Geosciences*, **15**, 47–56.

- 803 McIntyre, M. E., 1982: How well do we understand the dynamics of stratospheric warmings? *J.*
804 *Meteorol. Soc. Japan*, **60**, 37–65.
- 805 McPhaden, M., 2015: Playing hide and seek with el niño. *Nature Climate Change*, **5 (9)**, 791.
- 806 Ménesguen, C., A. Delpech, F. Marin, S. Cravatte, R. Schopp, and Y. Morel, 2019: Observations
807 and mechanisms for the formation of deep equatorial and tropical circulation. *Earth and Space*
808 *Science*.
- 809 Ménesguen, C., B. L. Hua, M. D. Fruman, and R. Schopp, 2009: Dynamics of the combined
810 extra-equatorial and equatorial deep jets in the atlantic. *J. Mar. Res.*, **67 (3)**, 323–346.
- 811 Montes, I., B. Dewitte, E. Gutknecht, A. Paulmier, I. Dadou, A. Oschlies, and V. Garçon, 2014:
812 High-resolution modeling of the eastern tropical pacific oxygen minimum zone: Sensitivity to
813 the tropical oceanic circulation. *J. Geophys. Res.: Oceans*, **119 (8)**, 5515–5532.
- 814 Morel, Y., J. Gula, and A. Ponte, 2019: Potential vorticity diagnostics based on balances between
815 volume integral and boundary conditions. *Accepted in Ocean Modelling*.
- 816 Müller, P., 2006: *The equations of oceanic motions*. Cambridge University Press.
- 817 Ollitrault, M., and A. Colin de Verdière, 2014: The ocean general circulation near 1000-m depth.
818 *J. Phys. Oceanogr.*, **44 (1)**, 384–409.
- 819 Ollitrault, M., and J.-P. Rannou, 2013: Andro: An argo-based deep displacement dataset. *Journal*
820 *of Atmospheric and Oceanic Technology*, **30 (4)**, 759–788.
- 821 Picaut, J., and R. Tournier, 1991: Monitoring the 1979-1985 equatorial pacific current transports
822 with expendable bathythermograph data. *J. Geophys. Res.: Oceans*, **96 (S01)**, 3263–3277.

- 823 Ponte, R. M., and J. Luyten, 1989: Analysis and interpretation of deep equatorial currents in the
824 central pacific. *J. Phys. Oceanogr.*, **19** (8), 1025–1038.
- 825 Qiu, B., S. Chen, and H. Sasaki, 2013a: Generation of the north equatorial undercurrent jets by
826 triad baroclinic rossby wave interactions. *J. Phys. Oceanogr.*, **43** (12), 2682–2698.
- 827 Qiu, B., T. Nakano, S. Chen, and P. Klein, 2017: Submesoscale transition from geostrophic flows
828 to internal waves in the northwestern pacific upper ocean. *Nature communications*, **8**, 14 055.
- 829 Qiu, B., D. L. Rudnick, S. Chen, and Y. Kashino, 2013b: Quasi-stationary north equatorial under-
830 current jets across the tropical north pacific ocean. *Geophys. Res. Lett.*, **40** (10), 2183–2187.
- 831 Reverdin, G., C. Frankignoul, E. Kestenare, and M. J. McPhaden, 1994: Seasonal variability in the
832 surface currents of the equatorial pacific. *J. Geophys. Res.: Oceans*, **99** (C10), 20 323–20 344.
- 833 Rhines, P., and W. Young, 1982: Homogenization of potential vorticity in planetary gyres. *J. Fluid*
834 *Mech.*, **122**, 347–367.
- 835 Rhines, P. B., 1975: Waves and turbulence on a beta-plane. *J. Fluid Mech.*, **69** (3), 417–443.
- 836 Ridgway, K., J. Dunn, and J. Wilkin, 2002: Ocean interpolation by four-dimensional weighted
837 least squares. application to the waters around australasia. *Journal of atmospheric and oceanic*
838 *technology*, **19** (9), 1357–1375.
- 839 Roemmich, D., and J. Gilson, 2009: The 2004–2008 mean and annual cycle of temperature, salin-
840 ity, and steric height in the global ocean from the argo program. *Progress in oceanography*,
841 **82** (2), 81–100.
- 842 Rowe, G. D., E. Firing, and G. C. Johnson, 2000: Pacific equatorial subsurface countercurrent
843 velocity, transport, and potential vorticity. *J. Phys. Oceanogr.*, **30** (6), 1172–1187.

844 Saout Grit, C., A. Ganachaud, C. Maes, L. Finot, L. Jamet, F. Baurand, and J. Grelet, 2015:
845 Calibration of ctd oxygen data collected in the coral sea during the 2012 bifurcation cruise.
846 *Mercator Ocean-Quarterly Newsletter*.

847 Stramma, L., P. Brandt, J. Schafstall, F. Schott, J. Fischer, and A. Körtzinger, 2008: Oxygen
848 minimum zone in the north atlantic south and east of the cape verde islands. *J. Geophys. Res.:
849 Oceans*, **113** (C4).

850 Stramma, L., S. Hüttl, and J. Schafstall, 2005: Water masses and currents in the upper tropical
851 northeast atlantic off northwest africa. *J. Geophys. Res.: Oceans*, **110** (C12).

852 Stramma, L., G. C. Johnson, E. Firing, and S. Schmidtko, 2010: Eastern pacific oxygen minimum
853 zones: Supply paths and multidecadal changes. *J. Geophys. Res.: Oceans*, **115** (C9).

854 Theiss, J., 2004: Equatorward energy cascade, critical latitude, and the predominance of cyclonic
855 vortices in geostrophic turbulence. *J. Phys. Oceanogr.*, **34** (7), 1663–1678.

856 Tsuchiya, M., 1975: Subsurface countercurrents in the eastern equatorial pacific ocean. *J. Mar.
857 Res.*, **33**, S145–S175.

858 Tsuchiya, M., 1981: The origin of the pacific equatorial 13 c water. *J. Phys. Oceanogr.*, **11** (6),
859 794–812.

860 Tsuchiya, M., R. Lukas, R. A. Fine, E. Firing, and E. Lindstrom, 1989: Source waters of the
861 pacific equatorial undercurrent. *Progress in Oceanography*, **23** (2), 101–147.

862 Uchida, H., G. Johnson, and K. McTaggart, 2010: Ctd oxygen sensor calibration procedures. Tech.
863 rep.

864 UNESCO-IOC, 2010: The international thermodynamic equation of seawater–2010: calculation
865 and use of thermodynamic properties.[includes corrections up to 31st october 2015]. Tech. rep.,
866 UNESCO.

867 Visbeck, M., 2002: Deep velocity profiling using lowered acoustic doppler current profilers: Bot-
868 tom track and inverse solutions. *Journal of Atmospheric and Oceanic Technology*, **19** (5), 794–
869 807.

870 Wyrtki, K., and B. Kilonsky, 1984: Mean water and current structure during the hawaii-to-tahiti
871 shuttle experiment. *J. Phys. Oceanogr.*, **14** (2), 242–254.

872 Youngs, M. K., and G. C. Johnson, 2015: Basin-wavelength equatorial deep jet signals across
873 three oceans. *J. Phys. Oceanogr.*, **45** (8), 2134–2148.

874 **LIST OF TABLES**

875 **Table 1.** Acronyms used for the denomination of the different currents. 42

876 **Table 2.** WOCE sections used for the study. Label for the L-ADCP data : a.: available,
877 p.a.: partially available, n.a.: not available. In bold: CASSIOPEE cruise. 43

878 **Table 3.** TAO sections used for the study sampled onboard Kaimimoana . Label for the
879 S-ADCP data : a.: available, n.a. : not available. 44

880 **Table 4.** Density layers used to target the first and second Tsuchiya jets in Fig-
881 ures 9 and 10. 45

TABLE 1. Acronyms used for the denomination of the different currents.

Short Name	Long Name	Direction	Depth
EUC	Equatorial Undercurrent	Eastward	thermocline
EIC	Equatorial Intermediate Current	Westward	$\simeq 500$ m
L-EIC	Lower Equatorial Intermediate Current	Westward	> 500 m
EDJ	Equatorial Deep Jets	Alternating	> 500 m
NSCC	Northern Subsurface Countercurrent	Eastward	$\simeq 350$ m
	Northern Tsuchiya Jet		
SSCC	Southern Subsurface Countercurrent	Eastward	$\simeq 350$ m
	Southern Tsuchiya Jet		
sSSCC	Secondary Southern Subsurface Countercurrent	Eastward	$\simeq 450$ m
	secondary Southern Tsuchiya Jet		
LLSCs	Low-Latitude Subsurface Currents	Alternating	thermocline - 600 m
LLICs	Low-Latitude Intermediate Currents	Alternating	> 700 m.

882 TABLE 2. WOCE sections used for the study. Label for the L-ADCP data : a.: available, p.a.: partially
883 available, n.a.: not available. In bold: CASSIOPEE cruise.

Section	Year	Dates	Longitude	Latitude range	Resolution	R/V	L-ADCP
P13	1992	04/08 - 21/10	165°E	5°S - 10°N	> 0.5°	JONH V. VICKERS	p.a.
P13	2011	15/05 - 26/08	165°E	5°S - 10°N	0.5°	RYOFU MARU	n.a.
P13	2015	18/07 - 24/08	165°E	10°S - 2°N	0.33°	L'ATALANTE	a.
P14	1993	05/07 - 02/09	179°W	15°S - 20°S	0.5°	TG THOMPSON	p.a.
P14	2007	08/10 - 20/11	179°W	15°S - 8°N	0.5°	MIRAI	n.a.
P15	2001	24/05 - 08/07	170°W	20°S - 10°S	0.5°	FRANKLIN	n.a.
P15	2009	03/02 - 24/03	170°W	20°S - 10°S	0.5°	SURVEYOR	n.a.
P15	2016	26/04 - 22/06	170°W	20°S - 0°	0.5°	INVESTIGATOR	a.
P16	1991	31/08 - 01/10	151°W	15°S - 5°N	0.5°	WASHINGTON	p.a.
P16	2006	13/02 - 29/03	151°W	5°S - 15°N	> 0.5°	TG THOMPSON	a.
P16	2015	10/04 - 13/05	151°W	15°S - 5°N	0.5°	RH BROWN	n.a.
P17	1991	31/05 - 11/07	135°W	5°S - 20°N	0.5°	WASHINGTON	p.a.
P18	1994	26/01 - 27/04	110°W	5°S - 20°N	0.5°	DISCOVER	p.a.
P18	2007	15/12/07 - 23/02/08	110°W	5°S - 20°N	0.5°	RH BROWN	a.
P18	2016	19/11 - 03/02	110°W	15°S - 5°N	0.5°	RH BROWN	a.

884 TABLE 3. TAO sections used for the study sampled onboard Kaimimoana . Label for the S-ADCP data : a.:
 885 available, n.a. : not available.

Name of the cruise	Dates	Longitude	Latitude range	Depth	Resolution	S-ADCP
GP1-06-KA	01/2006 - 02/2006	140°W	7.5°S- 9.5°N	1000 m	0.5°	a.
GP1-06-KA	01/2006 - 02/2006	125°W	7.5°S- 8.5°N	1000 m	0.5°	a.
GP2-06-KA	04/2006	110°W	7°S- 8°N	1000 m	0.5°	a.
GP2-06-KA	04/2006	95°W	4°S- 6°N	1000 m	0.5°	a.
GP3-04-KA	06/2004 - 07/2004	155°W	8°S- 9.5°N	1000 m	0.5°	a.
GP3-04-KA	06/2004 - 07/2004	140°W	7.5°S- 9.5°N	1000 m	0.5°	a.
GP3-06-KA	06/2006	170°W	8°S- 8°N	1000 m	0.5°	a.
GP3-06-KA	06/2006	155°W	8°S- 9.5°N	1000 m	0.5°	a.
GP5-04-KA	09/2004	140°W	2°S- 9°N	1000 m	0.5°	a.
GP5-04-KA	09/2004	125°W	8°S- 10°N	1000 m	0.5°	a.

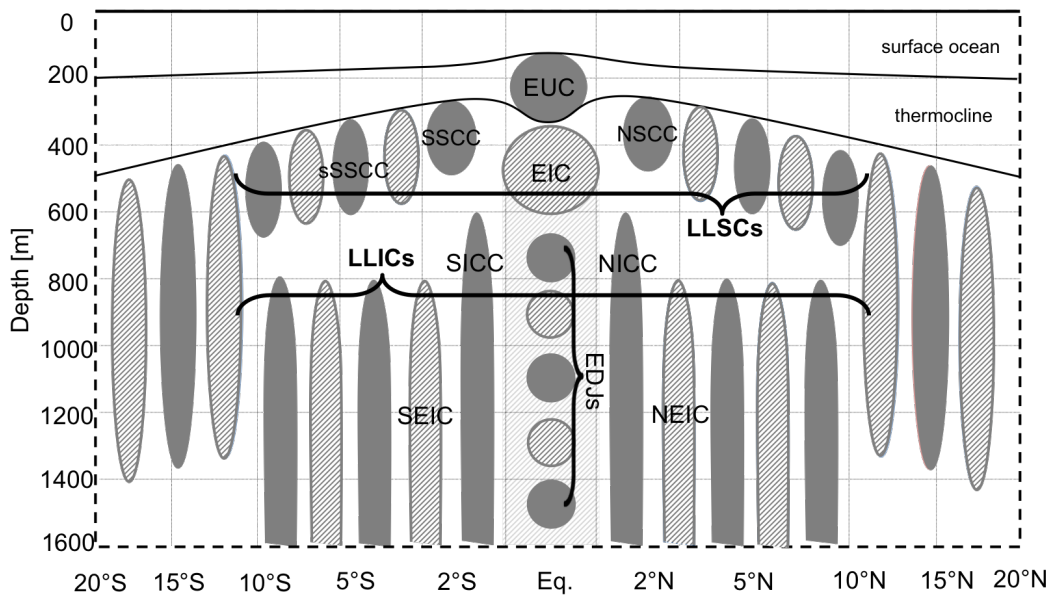
TABLE 4. Density layers used to target the first and second Tsuchiya jets in Figures 9 and 10.

Longitude	Density layer	Longitude	Density layer
170°W	1026.4 - 1026.8 kg m ⁻³	all	1027.15 - 1027.25 kg m ⁻³
155°W	1026.4 - 1026.8 kg m ⁻³		
140°W	1026.3 - 1026.7 kg m ⁻³		
125°W	1026.3 - 1026.6 kg m ⁻³		
110°W	1026.2 - 1026.6 kg m ⁻³		
95°W	1026.2 - 1026.4 kg m ⁻³		
Figure 9		Figure 10	

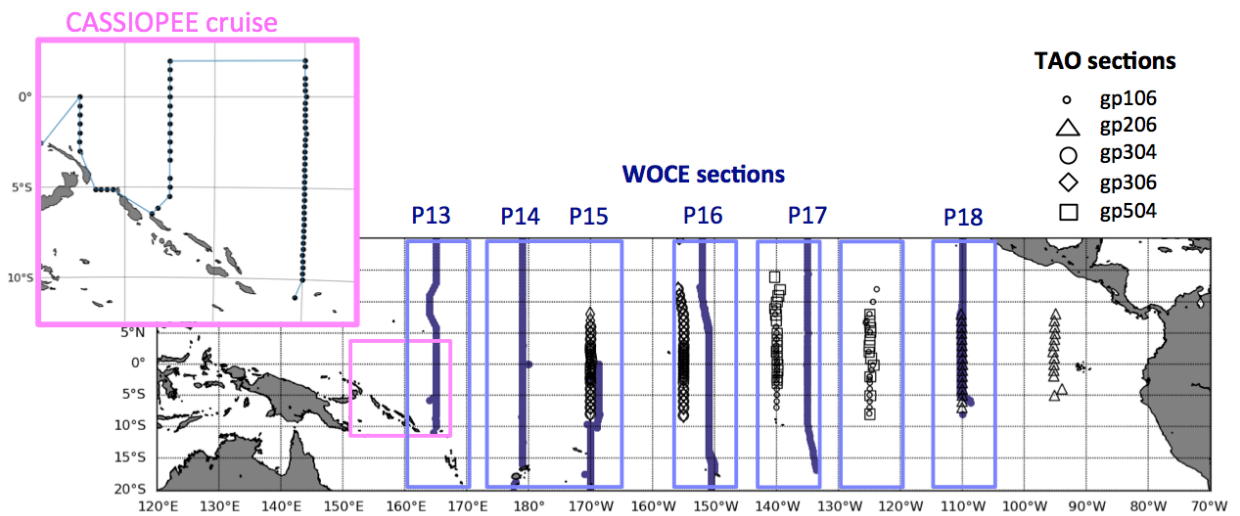
886 **LIST OF FIGURES**

- 887 **Fig. 1.** Schematic of the different zonal jets systems listed in Table 1 as a function of latitude and
 888 depth (in meters). Dark and light grey patches represent eastward and westward currents
 889 respectively. For the sake of simplicity, surface currents have not been represented. Adapted
 890 from Ménesguen et al. (2019). 48
- 891 **Fig. 2.** Cruise tracks used in this study. Blue lines represent the WOCE sections and their labels.
 892 Black symbols represent the different TAO cruises. The pink square box gives the detailed
 893 positions of the hydrological stations of the CASSIOPEE cruise. The blue square boxes
 894 represent the boxes used for Figure 10. 49
- 895 **Fig. 3.** (a) **CASSIOPEE zonal velocity sections** from L-ADCP measurements. Contours are every
 896 5 cm s^{-1} . Velocities are filtered in the vertical using an Hanning filter of 50 m. White con-
 897 tours represent density levels. Grey dashed line separate the two western boundary stations
 898 of section 157.5°E at 6°S and 6.5°S (Figure 2). (b) **Absolute geostrophic zonal velocity**
 899 **sections from CR17** (Cravatte et al. 2017) between the surface and 2000 m for the month
 900 of August. The colorbar is the same as the one used for (a). (c) **Comparison between**
 901 **CASSIOPEE (red) and Argo geostrophic zonal velocities (CR17)** within the isopycnal
 902 layer $1027.0\text{-}1027.6 \text{ kg m}^{-3}$ (approximately 500-1500 m). Light blue lines represent Argo
 903 geostrophic velocities for August and dark blue lines represent Argo annual mean veloci-
 904 ties. Velocities have been filtered using a running hanning mean of 1° of latitude. In (a), (b)
 905 and (c), left, middle and right panels correspond to sections 152.5°E , 157.5°E and 165°E
 906 respectively. 50
- 907 **Fig. 4.** **CASSIOPEE sections zoomed in between 0-800m.** (a) L-ADCP zonal velocity along
 908 the three sections of CASSIOPEE cruise: 152.5°E (left), 157.5°E (middle), 165°E (right).
 909 Contours are every 5 cm s^{-1} . Data have been filtered using a vertical Hanning filter over 50
 910 m. White lines represent density contours. (b) Same as (a) for oxygen. Contours are every
 911 $5 \mu\text{mol kg}^{-1}$. (c) Same as (a) for salinity. Contours are every 0.005 psu. Grey dashed line
 912 separate the two western boundary stations of section 157.5°E at 6°S and 6.5°S (Figure 2). 51
- 913 **Fig. 5.** **Tracer sections in CASSIOPEE.** (a) Oxygen concentration along the three sections of
 914 CASSIOPEE cruise: 152.5°E (left), 157.5°E (middle), 165°E (right). Contours are every 5
 915 $\mu\text{mol kg}^{-1}$. A vertical Hanning filter over 50 m has been applied. White lines are density
 916 contours. Grey dashed line separate the two western boundary stations of section 157.5°E at
 917 6°S and 6.5°S (Figure 2). (b) Same as (a) for salinity. Contours are every 0.05 psu. (c) Same
 918 as (a) for rescaled potential vorticity (see Section 2). Contours are every 0.2 s^{-1} . Note that
 919 the 152.5°E section could not be computed because it had a too small meridional extension
 920 for the computation of derivatives and rescaling. 52
- 921 **Fig. 6.** **Signature of EDJs in CASSIOPEE.** Vertical zonal velocity (black dashed lines) and oxy-
 922 gen concentration (gray solid lines) anomalies from 300 to 2800 m averaged between 1°N
 923 and 1°S at longitudes 152.5°E (left), 157.5°E (middle) and 165°E (right). Data have been
 924 filtered using a 100-500 m band-pass hanning filter in order to remove the large-scale varia-
 925 tion (over 500 m) and small scale noise (below 100 m). 53
- 926 **Fig. 7.** Meridional profiles of zonal jets and tracers averaged over isopycnal layers for the 165°E
 927 section of the CASSIOPEE cruise: L-ADCP zonal velocity (blue), oxygen (pale green),
 928 salinity (dark green) and rescaled potential vorticity (orange) computed as described in Sec-
 929 tion 2. The blue error bars indicate the standard deviation of the velocity within the isopycnal
 930 layer. The different layers are chosen to target the different jets observed : (a) First Tsuchiya
 931 jet ($1026.38 - 1026.67 \text{ kg m}^{-3}$), (b) Second Tsuchiya jet ($1026.8 - 1027.05 \text{ kg m}^{-3}$), (c)

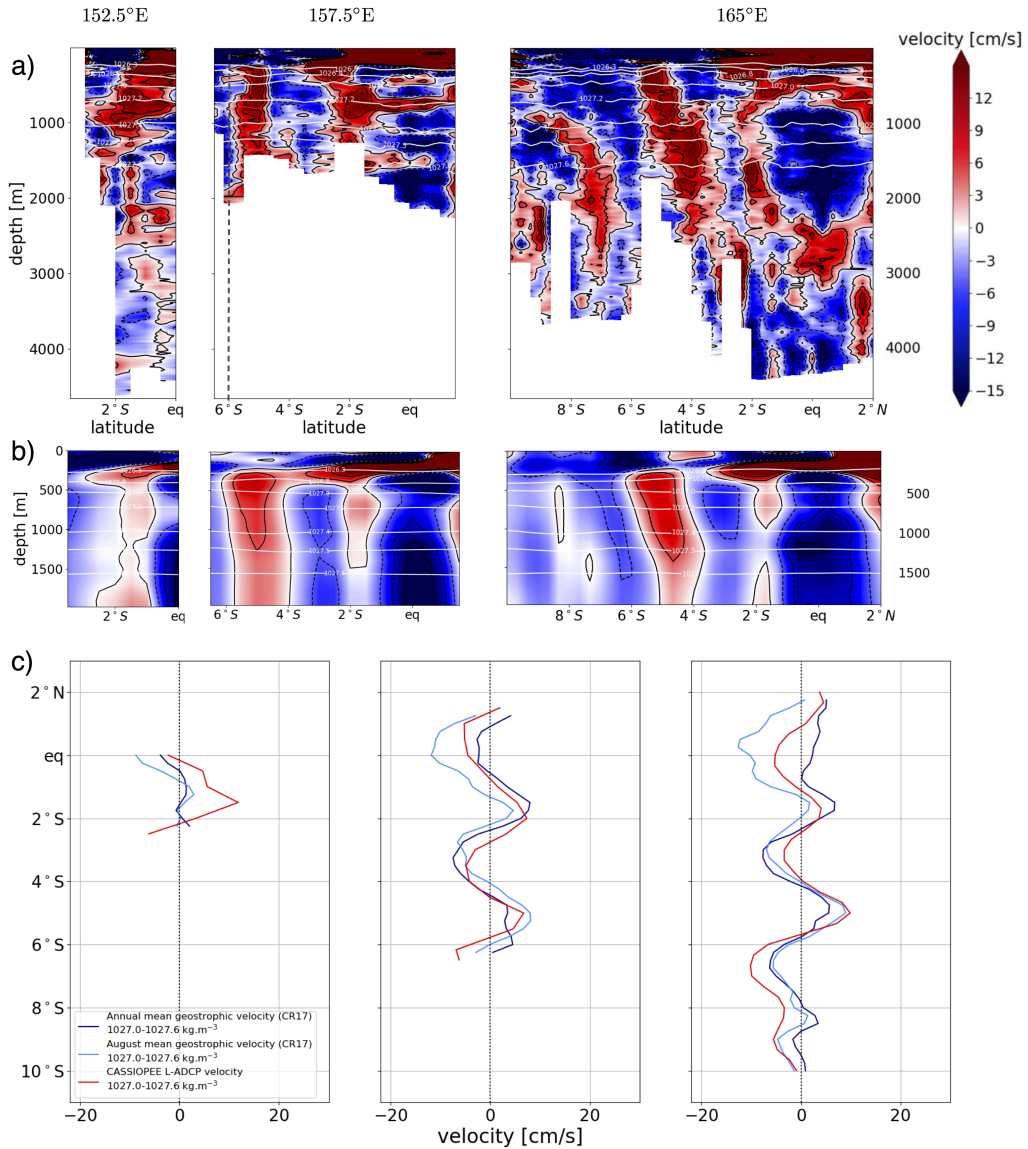
932	upper LLIC system ($1027.2 - 1027.4 \text{ kg m}^{-3}$), (d) lower LLIC system ($1027.49-1027.63$	
933	kg m^{-3}). Note that for the sake of clarity, potential vorticity and salinity axes are decreasing.	54
934	Fig. 8. Oxygen profiles in EDJs. Equatorial profiles of zonal velocity anomaly (coloured dashed	
935	lines) and oxygen concentration anomaly (colored solid lines) at the different WOCE lo-	
936	cations (Figure 2). Anomalies have been computed by using a 100-500 m bandpass filter.	
937	From left to right : P13 (165°E), P14 (180°) P15 (170°W), P16 (150°W), P17 (135°W) and	
938	P18 (110°W).	55
939	Fig. 9. Zonal evolution of tracers profiles in first and second Tsuchiya jets. TAO and WOCE	
940	sections averaged over isopycnal layers described in Table 4 for oxygen (upper panels)	
941	and salinity (lower panels). Coloured dashed lines represent velocity and solid lines rep-	
942	resent tracers. Symbols represent the positions of the northern and first and second southern	
943	Tsuchiya jets previously reported by Rowe et al. (2000). Black dashed lines connect the jet	
944	cores positions.	56
945	Fig. 10. Zonal evolution of tracers profiles in LLSC system. Meridional cruise sections at differ-	
946	ent longitudes across the tropical Pacific Ocean for oxygen (upper panels) and salinity (lower	
947	panels). From left to right: $160-170^\circ\text{E}$, $165-175^\circ\text{W}$, $145-155^\circ\text{W}$, $135-145^\circ\text{W}$, $120-130^\circ\text{W}$	
948	and $105-115^\circ\text{W}$. Coloured dashed and solid lines represent velocity and tracers associated	
949	with each cruise. Solid gray lines represent the mean geostrophic velocity from CR17 prod-	
950	uct averaged in the same longitude boxes. All data are averaged within the isopycnal layer	
951	$1027.15-1027.25 \text{ kg m}^{-3}$ (Table 4). The eastward jets on each side of the equator, indicated	
952	by black arrows on the left panel are the SICC and NICC.	57
953	Fig. 11. Tracers profiles in LLIC system. Upper panel : profiles of all WOCE cruises (Figure 2	
954	and Table 2) averaged in the isopycnic layer $1027.4 - 1027.5 \text{ kg m}^{-3}$ and filtered using	
955	meridional filter of 1.5° of the different properties: (a) oxygen, (b) zonal velocity from	
956	CR17 averaged from 165°E and 110°W , (c) salinity. Shaded regions in the background	
957	color indicate the location of eastward jets. Lower panel : Normalized meridional spectrum	
958	associated with these data. Thick dashed line : spectrum of the velocity (as described above),	
959	light grey lines: spectrum of each individual cruise tracer profile (d) oxygen, (e) salinity and	
960	solid black line : mean of all individual cruises spectra.	58
961	Fig. 12. Background tracer fields of oxygen (a)-(c) and salinity (b)-(d) from CSIRO Atlas of Re-	
962	gional Seas (Ridgway et al. 2002). (a) integration between isopycnals 1026.4 and 1026.9	
963	kg m^{-3} , typical layer for LLSCs, contours are every $10 \mu\text{mol kg}^{-1}$. (b) same as (a) but for	
964	salinity, contours are every 0.01 psu . (c) integration between isopycnals 1027.4 and 1027.6	
965	kg m^{-3} , typical layer for LLICs, contours are every $5 \mu\text{mol kg}^{-1}$. (d) same as (c) but for	
966	salinity, contours are every 0.001 psu .	59
967	Fig. 13. Background tracer field deformation in presence of physical processes. Left : map of the	
968	initial tracer field (dashed) and its deformation (solid) under physical processes associated	
969	with zonal jets (red). Right: meridional profiles of tracer field values (φ and its background	
970	value φ_0) and zonal velocities (U). (a) zonal advection in zonal background gradient. (b)	
971	zonal advection in slanting background gradient. (c) recirculation gyres and diffusion in	
972	meridional background gradient. (d) localized mixing in meridional background gradient	
973	(shaded areas represent mixing regions).	60



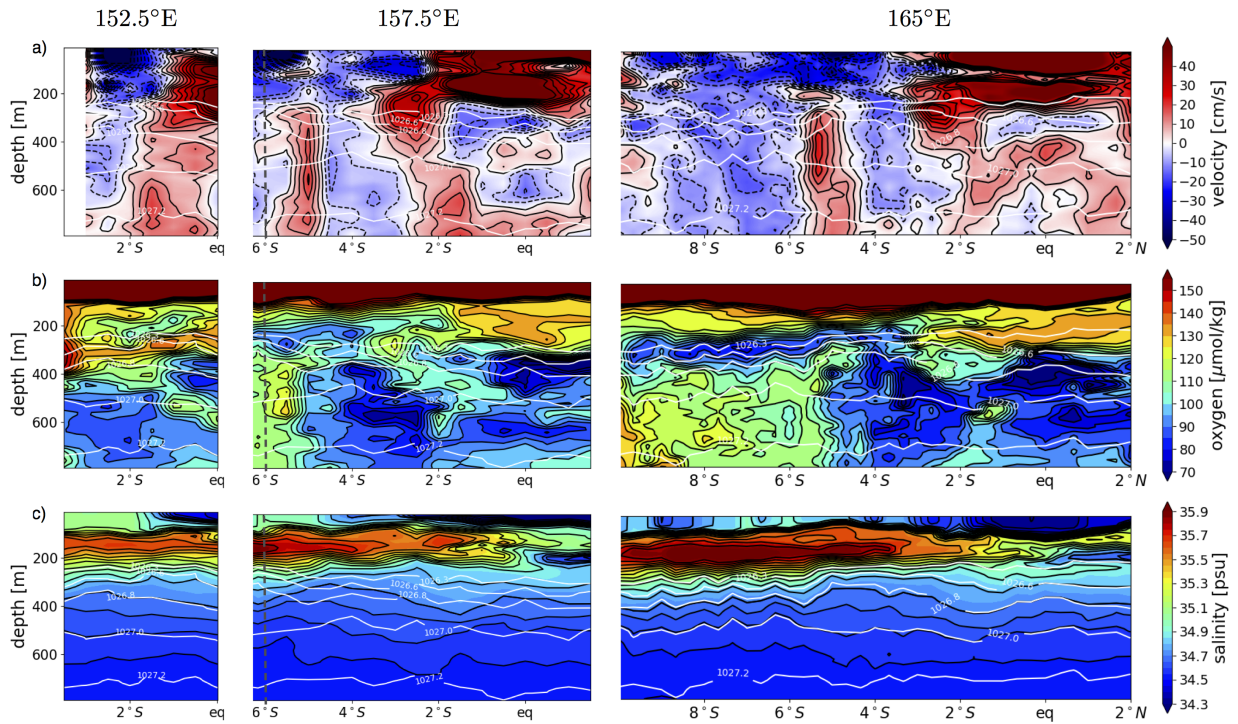
974 FIG. 1. Schematic of the different zonal jets systems listed in Table 1 as a function of latitude and depth (in
 975 meters). Dark and light grey patches represent eastward and westward currents respectively. For the sake of
 976 simplicity, surface currents have not been represented. Adapted from Ménesguen et al. (2019).



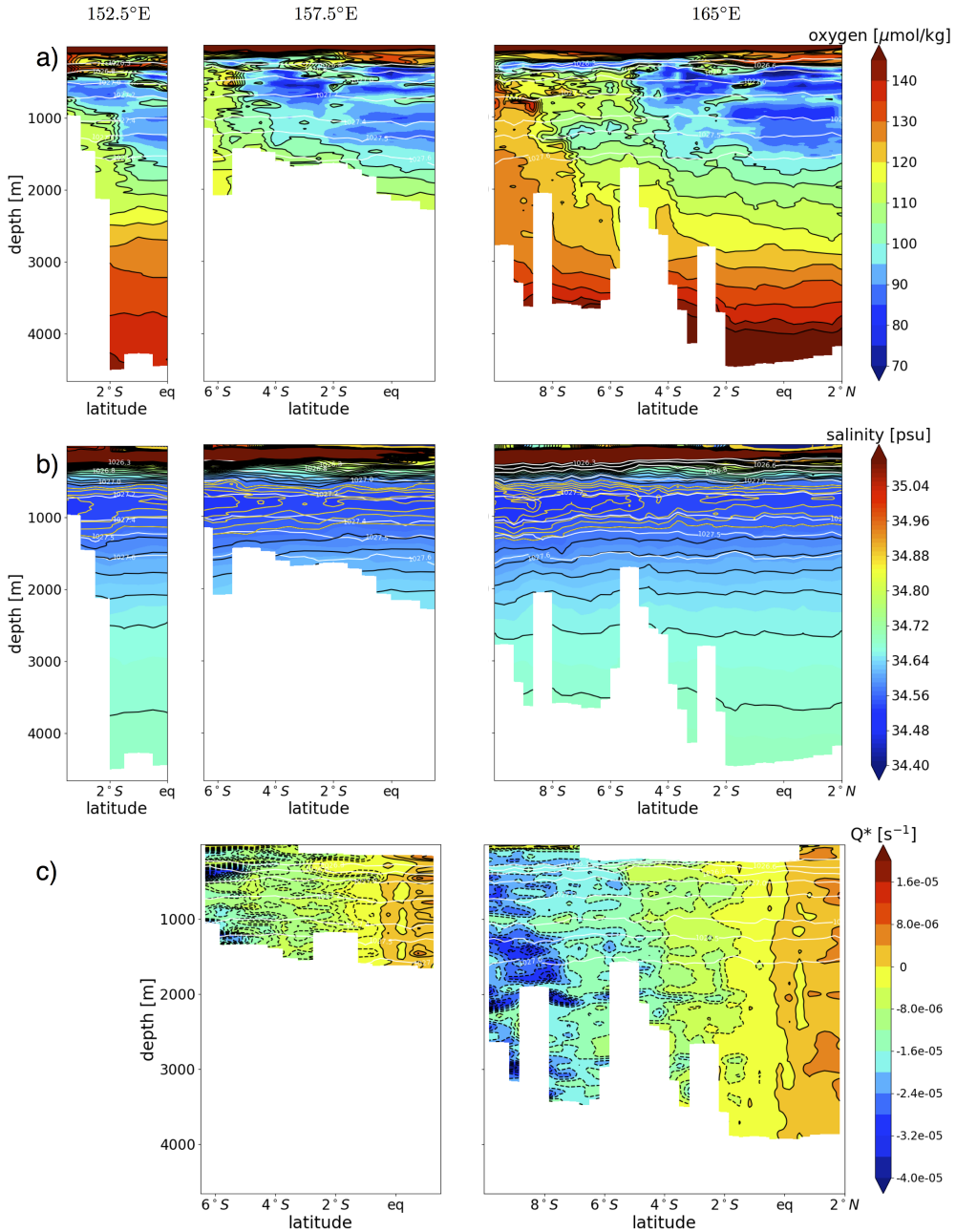
977 FIG. 2. Cruise tracks used in this study. Blue lines represent the WOCE sections and their labels. Black
 978 symbols represent the different TAO cruises. The pink square box gives the detailed positions of the hydrological
 979 stations of the CASSIOPEE cruise. The blue square boxes represent the boxes used for Figure 10.



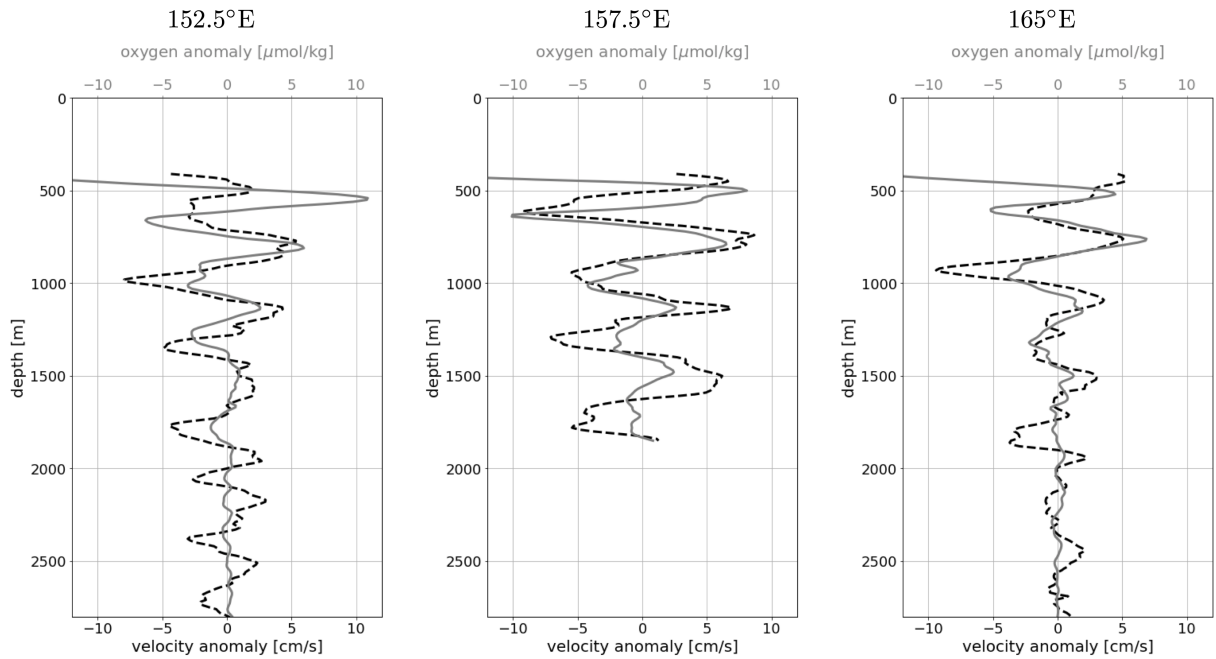
980 FIG. 3. (a) CASSIOPEE zonal velocity sections from L-ADCP measurements. Contours are every 5 cm s^{-1} .
 981 Velocities are filtered in the vertical using an Hanning filter of 50 m. White contours represent density levels.
 982 Grey dashed line separate the two western boundary stations of section 157.5°E at 6°S and 6.5°S (Figure 2).
 983 (b) Absolute geostrophic zonal velocity sections from CR17 (Cravatte et al. 2017) between the surface and
 984 2000 m for the month of August. The colorbar is the same as the one used for (a). (c) Comparison be-
 985 tween CASSIOPEE (red) and Argo geostrophic zonal velocities (CR17) within the isopycnal layer 1027.0-
 986 1027.6 kg m^{-3} (approximately 500-1500 m). Light blue lines represent Argo geostrophic velocities for August
 987 and dark blue lines represent Argo annual mean velocities. Velocities have been filtered using a running hanning
 988 mean of 1° of latitude. In (a), (b) and (c), left, middle and right panels correspond to sections 152.5°E, 157.5°E
 989 and 165°E respectively.



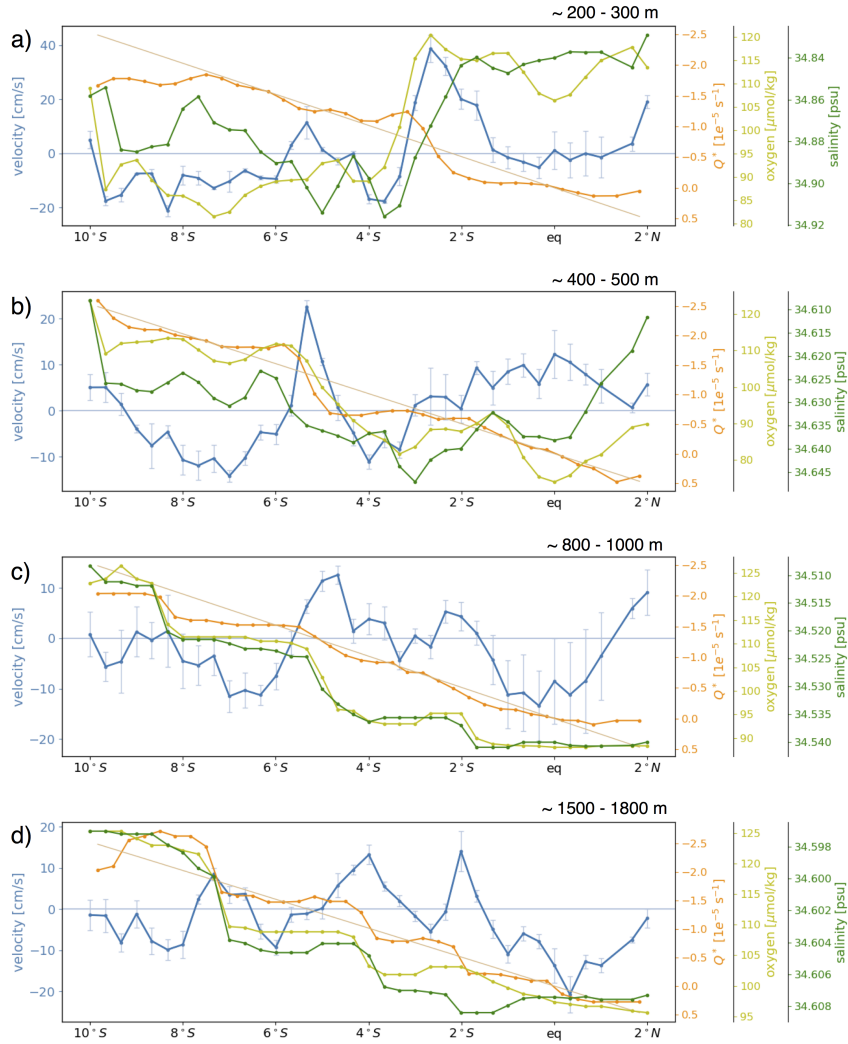
990 FIG. 4. **CASSIOPEE sections zoomed in between 0-800m.** (a) L-ADCP zonal velocity along the three
 991 sections of CASSIOPEE cruise: 152.5°E (left), 157.5°E (middle), 165°E (right). Contours are every 5 cm s⁻¹.
 992 Data have been filtered using a vertical Hanning filter over 50 m. White lines represent density contours. (b)
 993 Same as (a) for oxygen. Contours are every 5 μmol kg⁻¹. (c) Same as (a) for salinity. Contours are every 0.005
 994 psu. Grey dashed line separate the two western boundary stations of section 157.5°E at 6°S and 6.5°S (Figure 2).



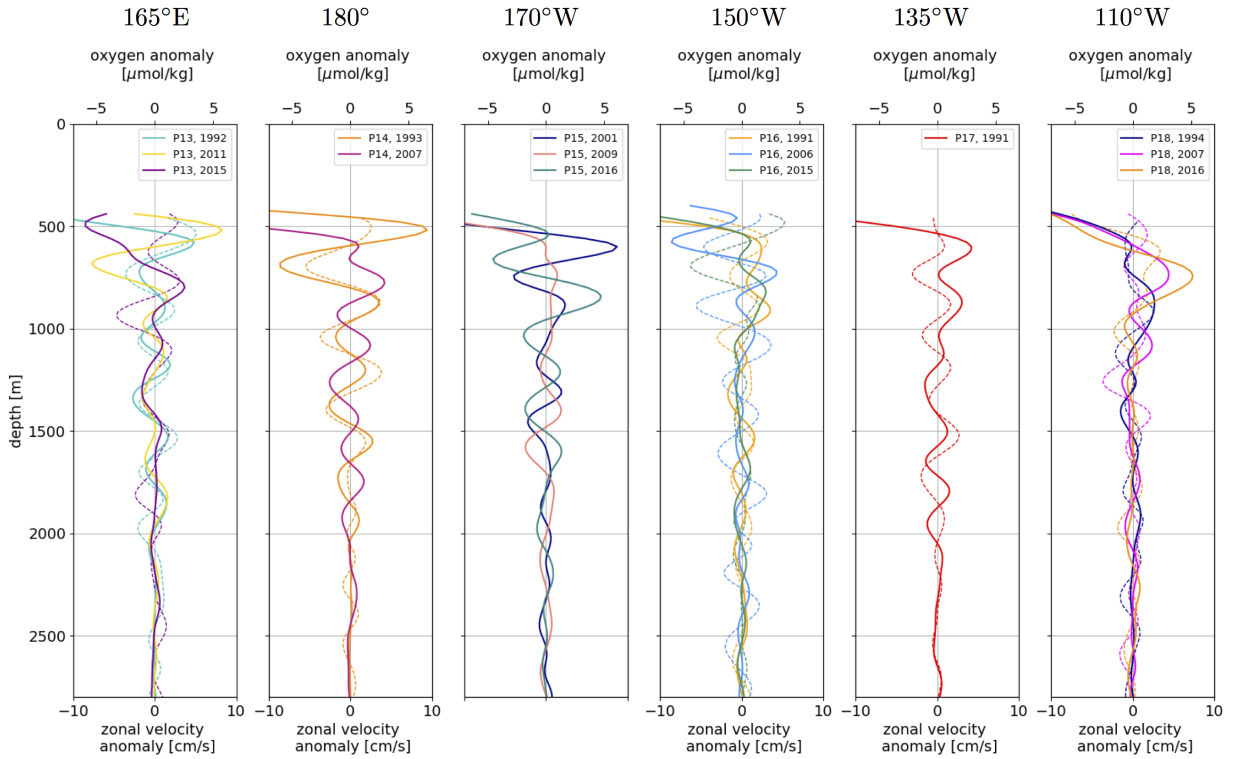
995 **FIG. 5. Tracer sections in CASSIOPEE.** (a) Oxygen concentration along the three sections of CASSIOPEE
 996 cruise: 152.5°E (left), 157.5°E (middle), 165°E (right). Contours are every 5 $\mu\text{mol kg}^{-1}$. A vertical Hanning
 997 filter over 50 m has been applied. White lines are density contours. Grey dashed line separate the two western
 998 boundary stations of section 157.5°E at 6°S and 6.5°S (Figure 2). (b) Same as (a) for salinity. Contours are every
 999 0.05 psu. (c) Same as (a) for rescaled potential vorticity (see Section 2). Contours are every 0.2 s^{-1} . Note that
 1000 the 152.5°E section could not be computed because it had a too small meridional extension for the computation
 1001 of derivatives and rescaling.



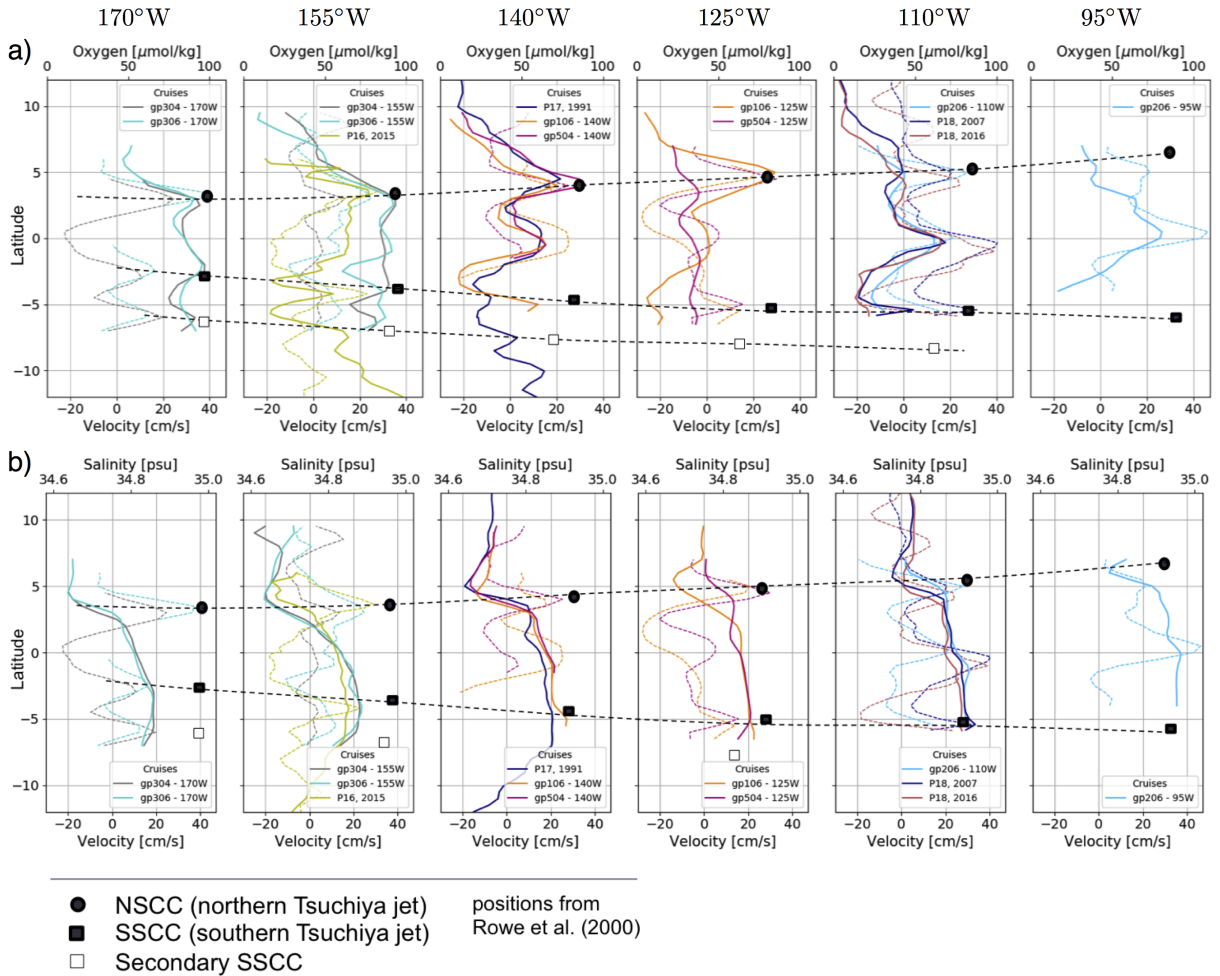
1002 **FIG. 6. Signature of EDJs in CASSIOPEE.** Vertical zonal velocity (black dashed lines) and oxygen concen-
 1003 tration (gray solid lines) anomalies from 300 to 2800 m averaged between 1°N and 1°S at longitudes 152.5°E
 1004 (left), 157.5°E (middle) and 165°E (right). Data have been filtered using a 100-500 m band-pass hanning filter
 1005 in order to remove the large-scale variation (over 500 m) and small scale noise (below 100 m).



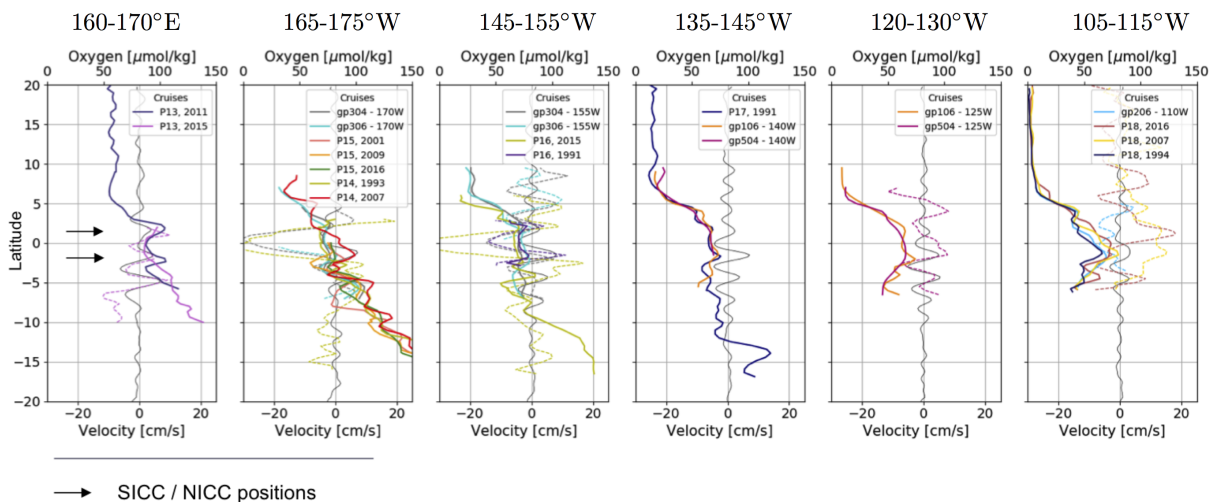
1006 FIG. 7. Meridional profiles of zonal jets and tracers averaged over isopycnal layers for the 165°E section of
 1007 the CASSIOPEE cruise: L-ADCP zonal velocity (blue), oxygen (pale green), salinity (dark green) and rescaled
 1008 potential vorticity (orange) computed as described in Section 2. The blue error bars indicate the standard deviation
 1009 of the velocity within the isopycnal layer. The different layers are chosen to target the different jets observed
 1010 : (a) First Tsuchiya jet ($1026.38 - 1026.67 \text{ kg m}^{-3}$), (b) Second Tsuchiya jet ($1026.8 - 1027.05 \text{ kg m}^{-3}$), (c) up-
 1011 per LLIC system ($1027.2 - 1027.4 \text{ kg m}^{-3}$), (d) lower LLIC system ($1027.49-1027.63 \text{ kg m}^{-3}$). Note that for
 1012 the sake of clarity, potential vorticity and salinity axes are decreasing.



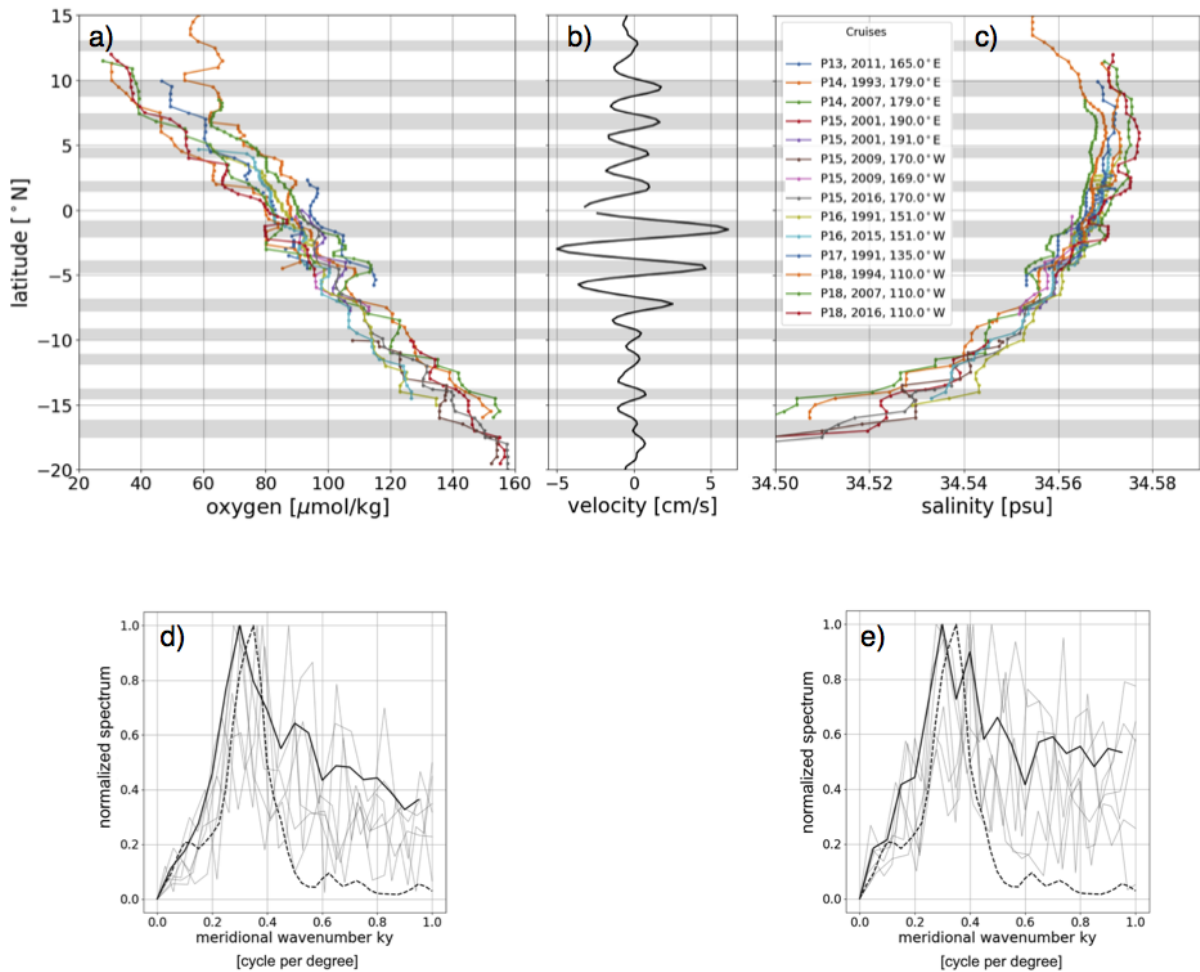
1013 **FIG. 8. Oxygen profiles in EDJs.** Equatorial profiles of zonal velocity anomaly (coloured dashed lines) and
 1014 oxygen concentration anomaly (colored solid lines) at the different WOCE locations (Figure 2). Anomalies have
 1015 been computed by using a 100-500 m bandpass filter. From left to right : P13 (165°E), P14 (180°) P15 (170°W),
 1016 P16 (150°W), P17 (135°W) and P18 (110°W).



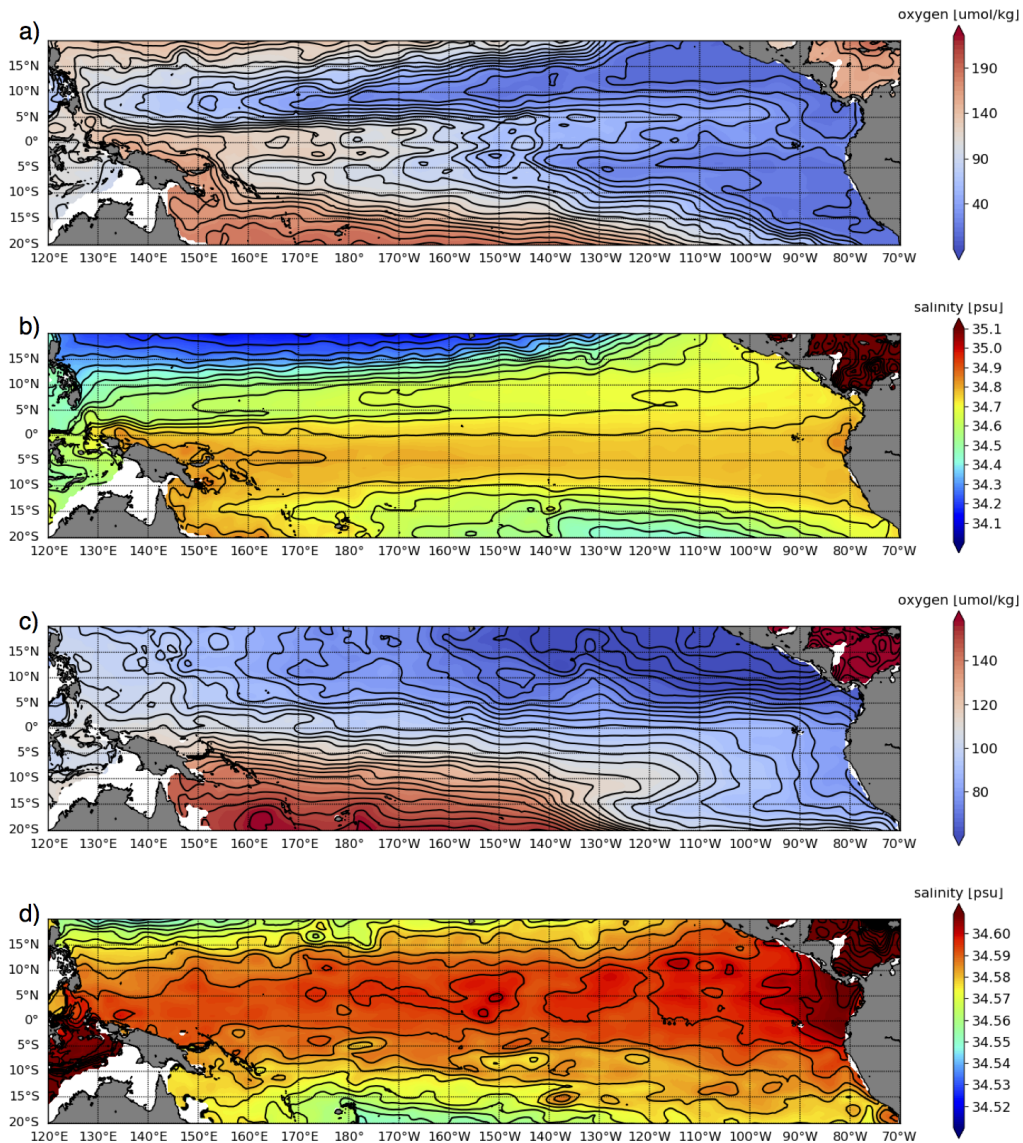
1017 FIG. 9. Zonal evolution of tracers profiles in first and second Tsuchiya jets. TAO and WOCE sec-
 1018 tions averaged over isopycnal layers described in Table 4 for oxygen (upper panels) and salinity (lower panels).
 1019 Coloured dashed lines represent velocity and solid lines represent tracers. Symbols represent the positions of the
 1020 northern and first and second southern Tsuchiya jets previously reported by Rowe et al. (2000). Black dashed
 1021 lines connect the jet cores positions.



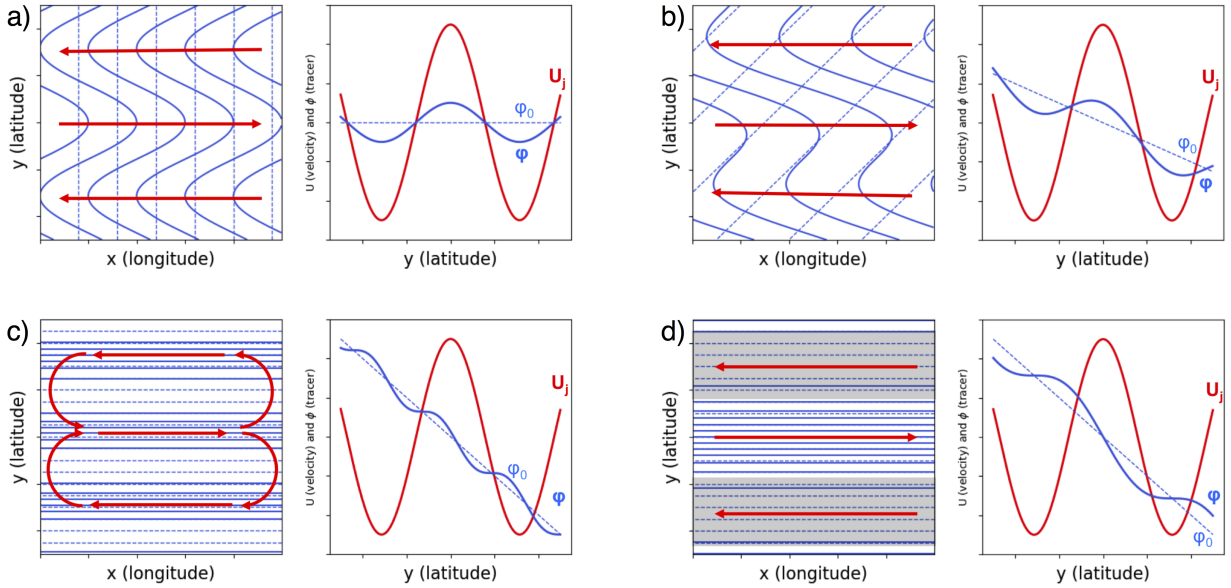
1022 **FIG. 10. Zonal evolution of tracers profiles in LLSC system.** Meridional cruise sections at different longi-
 1023 tudes across the tropical Pacific Ocean for oxygen (upper panels) and salinity (lower panels). From left to right:
 1024 160-170°E, 165-175°W, 145-155°W, 135-145°W, 120-130°W and 105-115°W. Coloured dashed and solid lines
 1025 represent velocity and tracers associated with each cruise. Solid gray lines represent the mean geostrophic veloc-
 1026 ity from CR17 product averaged in the same longitude boxes. All data are averaged within the isopycnal layer
 1027 $1027.15\text{-}1027.25 \text{ kg m}^{-3}$ (Table 4). The eastward jets on each side of the equator, indicated by black arrows on
 1028 the left panel are the SICC and NICC.



1029 **FIG. 11. Tracers profiles in LLIC system.** Upper panel : profiles of all WOCE cruises (Figure 2 and Table 2)
 1030 averaged in the isopycnic layer $1027.4 - 1027.5 \text{ kg m}^{-3}$ and filtered using meridional filter of 1.5° of the different
 1031 properties: (a) oxygen, (b) zonal velocity from CR17 averaged from 165°E and 110°W , (c) salinity. Shaded
 1032 regions in the background color indicate the location of eastward jets. Lower panel : Normalized meridional
 1033 spectrum associated with these data. Thick dashed line : spectrum of the velocity (as described above), light
 1034 grey lines: spectrum of each individual cruise tracer profile (d) oxygen, (e) salinity and solid black line : mean
 1035 of all individual cruises spectra.



1036 FIG. 12. **Background tracer fields** of oxygen (a)-(c) and salinity (b)-(d) from CSIRO Atlas of Regional Seas
 1037 (Ridgway et al. 2002). (a) integration between isopycnals 1026.4 and 1026.9 kg m^{-3} , typical layer for LLSCs,
 1038 contours are every $10 \mu\text{mol kg}^{-1}$. (b) same as (a) but for salinity, contours are every 0.01 psu . (c) integration
 1039 between isopycnals 1027.4 and 1027.6 kg m^{-3} , typical layer for LLICs, contours are every $5 \mu\text{mol kg}^{-1}$. (d)
 1040 same as (c) but for salinity, contours are every 0.001 psu .



1041 **FIG. 13. Background tracer field deformation in presence of physical processes.** Left : map of the initial
 1042 tracer field (dashed) and its deformation (solid) under physical processes associated with zonal jets (red). Right:
 1043 meridional profiles of tracer field values (ϕ and its background value ϕ_0) and zonal velocities (U). (a) zonal
 1044 advection in zonal background gradient. (b) zonal advection in slanting background gradient. (c) recirculation
 1045 gyres and diffusion in meridional background gradient. (d) localized mixing in meridional background gradient
 1046 (shaded areas represent mixing regions).